

3D modeling in Petrel of geological CO₂ storage site

3D modellering i Petrel av geologiskt CO₂
lagringsområde

Niklas Gunnarsson

ABSTRACT

3D modeling in Petrel of geological CO₂ storage site

Niklas Gunnarsson

If mitigation measures are not made to prevent global warming the consequences of a continued global climate change, caused by the use of fossil fuels, may be severe. Carbon Capture and Storage (CCS) has been suggested as a way of decreasing the global atmospheric emission of CO₂. In the realms of MUSTANG, a four year (2009-2013) large-scale integrating European project funded by the EU FP7, the objective is to gain understanding of the performance as well as to develop improved methods and models for characterizing so-called saline aquifers for geological storage of CO₂. In this context a number of sites of different geological settings and geographical locations in Europe are also analyzed and modeled in order to gain a wide understanding of CO₂ storage relevant site characteristics. The south Scania site is included into the study as one example site with data coming from previous geothermal and other investigations. The objective of the Master's thesis work presented herein was to construct a 3D model for the south Scania site by using modeling/simulation software Petrel, evaluate well log data as well as carry out stochastic simulations by using different geostatistical algorithms and evaluate the benefits in this. The aim was to produce a 3D model to be used for CO₂ injection simulation purposes in the continuing work of the MUSTANG project.

The sequential Gaussian simulation algorithm was used in the porosity modeling process of the Arnager greensand aquifer with porosity data determined from neutron and gamma ray measurements. Five hundred realizations were averaged and an increasing porosity with depth was observed.

Two different algorithms were used for the facies modeling of the alternative multilayered trap, the truncated Gaussian simulation algorithm and the sequential indicator simulation algorithm. It was seen that realistic geological models were given when the truncated Gaussian simulation algorithm was used with a low-nugget variogram and a relatively large range.

Keywords: CO₂ sequestration, Petrel, Sequential Gaussian simulation, Truncated Gaussian simulation, Sequential indicator simulation, Porosity modeling, Facies modeling, Variogram analysis, South Scania site.

*Department of Earth Sciences, Uppsala University, Villavägen 16, SE-752 36 Uppsala
ISSN 1401-5765*

REFERAT

3D modellering i Petrel av geologiskt CO₂ lagringsområde

Niklas Gunnarsson

Den antropogena globala uppvärmningen orsakad av användandet av fossila bränslen kan få förödande konsekvenser om ingenting görs. Koldioxidavskiljning och lagring är en åtgärd som föreslagits för att minska de globala CO₂-utsläppen. Inom ramarna för MUSTANG, ett fyra år långt (2009-2013) integrerande projekt finansierat av EU FP7 (www.co2mustang.eu), utvecklas metoder, modeller och förståelse angående så kallade saltvattenakviferers lämplighet för geologisk koldioxidlagring. En del av projektet är att analysera ett antal representativa formationer i olika delar av Europa för att få kunskap angående förekommande koldioxidlagringsspecifika egenskaper hos saltvattenakviferer. Ett av områdena som har inkluderats är i sydvästra Skåne. Syftet med detta examensarbete var att konstruera en 3D modell över detta område med hjälp av modellerings/simuleringsprogrammet Petrel, utvärdera borrhålsdata samt genomföra stokastiska simuleringar med olika geostatistiska algoritmer och utvärdera dem. Målsättningen var att konstruera en modell för CO₂ injiceringssimuleringar i det forstsatta arbetet inom MUSTANG-projektet.

En algoritm av sekventiell Gaussisk typ användes vid porositetsmodelleringen av Arnager Grönsandsakviferen med porositetsdata erhållen från neutron- och gammastrålningsmätningar. Ett genomsnitt av femhundra realisationer gjordes och en porositetstrend som visade en ökning med djupet kunde åskådliggöras.

Två olika algoritmer användes vid faciesmodelleringen av den alternativa flerlagrade fällan: en algoritm av trunkerade Gaussisk typ och en sekventiell indikatorsimuleringsalgoritm. Resultaten tyder på att en realistisk geologisk modell kan erhållas vid användandet av den trunkerande algoritmen med ett låg-nugget variogram samt en förhållandevis lång range.

Nyckelord: CO₂ lagring, Petrel, Sekventiell Gaussisk simulering, Trunkerad Gaussisk simulering, Sekventiell indikator simulering, Porositetsmodellering, Faciesmodellering, Variogramanalys, Sydvästra Skåne

PREFACE

This Master thesis (30 ECTS) is the final step in order to graduate with a Master of science degree in *Environmental and Aquatic engineering* at Uppsala University, Sweden and was carried out in the realms of four year (2009-2013) large-scale integrating European project *MUSTANG* funded by the EU FP7 aiming at developing guidelines, methods and tools for the characterization of deep saline aquifers for long term storage of CO₂. Subject reviewer was assistant Professor Fritjof Fagerlund, thesis examiner was Professor Allan Rodhe, supervisor was the main coordinator of MUSTANG project Professor Auli Niemi and co-supervisor was PhD student Kristina Rasmusson.

I would like to thank my supervisor Auli Niemi for all the help and support making this thesis possible. I would like to thank Kristina Rasmusson for helpful advices and suggestions. I would like to thank Dr. Mikael Erlström at SGU for giving valuable insights as well as providing data. I would also like to thank E.ON Sweden, especially Björn Möller who has been the contact person, for providing their data for this work. I would like to thank Schlumberger for providing the Petrel code and the people at Schlumberger for their quick and helpful replies on Petrel-related issues and providing the technical manual. Lastly I would also like to thank the people at Thunderhead engineering for all the support on PetraSIM even though those simulations did not make it to the final report.

Uppsala, 2011

Niklas Gunnarsson

Copyright © Niklas Gunnarsson and Department of Earth Sciences, Air, Water and Landscape Science, Uppsala University.

UPTEC W 11 029, ISSN 1401-5765

Printed at the Department of Earth Sciences, Geotryckeriet, Uppsala University, Uppsala, 2011.

POPULAR SCIENCE REVIEW

3D modeling in Petrel of geological CO₂ storage site

Niklas Gunnarsson

Global warming has been on the world agenda for some time now. It is claimed that the increase of atmospheric CO₂ due to the burning of fossil fuels is the reason. The consequences of global warming might be many and severe. Global warming might lead to polar ices melting resulting in the sea level rising, a scenario devastating for coastal areas around the world and particularly for small island nations. Global warming might also lead to an increase in droughts, a difficult situation for countries for example in eastern Africa already frequently troubled by droughts. Some researchers say that the effects of global warming already can be seen and others claim that the changes being observed are part of a natural climate cycle with some periods naturally being warmer than others.

Whether global warming is real or not investments all over the world are made to reduce our dependence on fossil fuels by expansion on renewable energy sources such as wind, sun and hydropower. It has not come to the stage however where renewable energy sources completely can replace fossil fuels. It is here that Carbon Capture and Storage (CCS) plays an important role. CCS has been suggested as a measure to decrease global CO₂ emission. CCS is the process where carbon is captured in the process of burning a fossil fuel for energy extraction, it is then transported and stored at a suitable location. Several storage locations have been discussed among them ocean and geological storage. Geological storage where the CO₂ is injected into the bedrock is the most common one and will be the point of focus in this thesis.

The geological storage location must have some characteristic properties. First of all it must lay deep, at a certain depth and temperature where CO₂ becomes supercritical. The density of supercritical CO₂ is higher than that of gaseous CO₂ increasing storage efficiency. The bedrock where the CO₂ is injected must be highly permeable and above the injection section an impermeable layer called a cap rock must exist hindering the CO₂ leaking upwards and out.

When the CO₂ has been injected into the bedrock there are several trapping mechanisms, the first is the physical entrapment which is when the impermeable cap rock prevents the CO₂ rising upwards. After a while the CO₂ starts reacting with existing bedrock minerals and finally the CO₂ mineralizes itself, this last process may take several thousand years. CCS has been criticized with the objection that it only prolongs our dependence on fossil fuels and that we in fact should be focusing on finding renewable energy sources instead of relying on fossil fuels that sooner or later will run out. Another objection to it is the uncertainty of the storage, leakage might occur.

The site investigated in this thesis was the south Scania site, one of a number of sites analyzed in the MUSTANG project where the objective is to gain understanding on so-called saline aquifers, the main candidate formations for geological storage of CO₂. The data used for this

project was provided by SGU, originally collected by E.ON in e.g. earlier geothermal investigations and consisted of geophysical as well as borehole data. The aim of this thesis was to analyze the geostatistical characteristics of this data, to develop a 3D structural model, carry out porosity modeling as well as carry out facies modeling with two different simulation algorithms comparing the results.

The structural 3D model was developed with Petrel software, a common 3D modeling and simulation tool in the oil and gas industry produced by Schlumberger. The development of the 3D structural model consisted of several steps including creation of geological horizons, layers and grid discretization, a grid dividing a 3D model into small boxes called grid cells.

Porosity modeling was carried out for the secondary trap also referred to as the Arnager greensand aquifer, one particular lateral section that initial drillings and investigations has shown to be suitable for CO₂ storage. It could be seen that the average porosity was quite high and increased with depth. A simulation algorithm called the sequential Gaussian simulation algorithm (*sgsim*) was used in populating the grid cells. An algorithm is a step by step procedure to solve a certain problem and the *sgsim* is one of the most common simulation algorithm in this kind of modeling. One algorithm-run results in one "realization" which is one possible outcome honoring input data and geostatistical conditions, however several runs is to prefer thus 500 realizations were averaged. One drawback in the porosity modeling was the fact that only data from one borehole was at hand. For more precise modeling porosity data from several wells should be gathered.

Facies modeling was carried out for the alternative multilayered trap where four facies (rock characteristics) had been identified: claystone, siltstone, fine grained sandstone and medium grained sandstone. For the facies modeling two types of simulation algorithms were used, the truncated Gaussian simulation algorithm (*gtsim*) and the sequential indicator simulation algorithm (*sisim*).

Two types of *gtsim* simulations were made, one with a computed vertical variogram and one with a default variogram. A variogram describes the spatial variance between two sample points. From the variogram, the nugget can be held which is the variance between two measured points very close to each other. The range is the distance where the variance between two measured points is at a maximum. From discussions with a state geologist it was understood that an order sequence existed between the different facies with claystone followed by siltstone followed by fine grained sandstone followed by medium grained sandstone. The *gtsim* honored this condition when the default vertical variogram was used with a large range. When the *gtsim* was used with the computed variogram that had a quite high nugget, this order relation was not honored. For the generation of a realistic geological model for the alternative multilayered trap the nugget being used must be very low and the horizontal range quite high otherwise the facies order is not honored.

When using the sequential indicator simulation a variogram for each facies could be used honoring more detail of the data. However the drawback with *sisim* was that the order relation was not honored thus resulting in an unrealistic geological model.

POPULÄRVETENSKAPLIG SAMMANFATTNING

3D modellering i Petrel av geologiskt CO₂ lagringsområde

Niklas Gunnarsson

Användandet av fossila bränslen och de stora CO₂ utsläppen anses vara orsaken till vår tids största kris, global uppvärmning och klimatförändring. Konsekvenserna av den globala uppvärmningen kan bli mycket svåra, bland annat befarar vissa forskare att havsnivån stiger då polarisarna börjat smälta, ett förödande scenario för kustområden runt om i världen och i synnerhet för små ö-nationer. En global uppvärmning kan också leda till att länder i till exempel östra Afrika oftare drabbas av torka. Vissa forskare menar att effekterna av den globala uppvärmningen redan kan ses men andra hävdar att förändringarna som observerats är en del av en naturlig klimatcykel med vissa perioder naturligt varmare än andra.

Oavsett om den globala uppvärmningen är verklig eller inte görs investeringar över hela världen för att minska vårt beroende av fossila bränslen genom satsningar på förnyelsebara energikällor som vind, sol och vattenkraft. Än så länge kan de förnyelsebara energikällorna inte helt ersätta de fossila bränslena. Det är här som Carbon Capture and Storage (CCS) kommer in i bilden. CCS har föreslagits som en åtgärd för att minska de globala CO₂ utsläppen och är en samlingsterm för den process där koldioxiden separeras från ett fossilt bränsle för att sedan transporteras till en lämplig plats där det slutligen lagras. Olika lagringsmetoder finns, bland annat så kallad geologisk lagring där CO₂ injiceras ner i berggrunden. Det är denna typ av lagring som denna rapport kommer att fokusera på.

Den geologiska lagringsplatsen måste ha vissa karakteristiska egenskaper. Först och främst måste lagerföljden vara djupt belägen då CO₂ blir superkritiskt på ett visst djup och vid en viss temperatur. Superkritiskt CO₂ har högre densitet än CO₂ i gasform vilket ökar lagringskapaciteten. Berggrunden där CO₂ injiceras måste ha en hög permeabilitet och ovanför det permeabla injiceringsskiktet måste det finnas en icke permeabel takbergart som hindrar koldioxiden att stiga upp genom berggrunden och ut i atmosfären.

När CO₂ har injicerats i berggrunden finns flera mekanismer för att förhindra läckage. Den första mekanismen är när det ogenomträngliga taket hindrar koldioxiden att stiga uppåt. Koldioxiden kommer sedan efter ett tag att börja reagera med mineraler i berggrunden och slutligen bli ett mineral självt, en process som kan ta flera tusen år. CCS har kritiserats med argument som att det bara förlänger vårt beroende av fossila bränslen och att fokus istället borde ligga på att utveckla nya och befintliga förnyelsebara energikällor i stället för att förlita oss på fossila bränslen som förr eller senare tar slut. En annan invändning mot CCS är osäkerheten kring själva lagringen då risken för läckage finns.

Den lagringsplats som undersöktes i detta examensarbete ligger i sydvästra Skåne och är en av flera platser som undersöks inom MUSTANG-projektet med målet att få en ökad kunskap om så kallade saltvattenakviferer, den typ av formationer med störst global lagringspotential. Datan som användes bestod av geofysisk data samt borrhålsdata och erhöles av SGU som i sin tur erhållit den av E.ON som samlat in den under bland annat geotermiska undersökningar.

Syftet med detta examensarbete var att analysera den geostatistiska datan, utveckla en strukturell 3D modell, genomföra porositetsmodelleringar samt faciesmodelleringar med olika simuleringsalgoritmer och utvärdera resultaten.

Den strukturella 3D modellen utvecklades i Petrel, ett 3D modellerings-/simuleringsverktyg som används främst inom olje- och gasindustrin tillverkat av Schlumberger. En 3D modell består av ett rutnät indelat i små lådor som kallas celler. Konstruerandet av den strukturella 3D modellen bestod av flera steg, inklusive skapandet av geologiska horisonter och rutnätsindelning.

Porositet är enkelt uttryckt ett begrepp för hur mycket hålrum ett material har och porositetsmodellering utfördes för en lagerföljd vid namn Arnager Grönsandsakviferen. Inledande borrhningar och undersökningar har givit indikationer om denna lagerföljds lämplighet för CO₂ lagring. Den genomsnittliga porositeten för lagerföljden var hög och ökade med djupet. En simuleringsalgoritm av sekventiell Gaussisk typ (*sgsim*) användes vid porositetsmodelleringen. En algoritm är en stegvis procedur för att lösa ett visst problem och *sgsim* är en av de vanligaste simuleringsalgoritmerna vid denna typ av modellering. En algoritmkörning resulterar i en realisering, dvs. ett möjligt utfall. Flera körningar är dock att föredra och således genererades 500 realiseringar och ett genomsnitt av dessa beräknades. En svaghet i porositetsmodelleringarna var det faktum att endast data från ett borrhål fanns att tillgå. För en bättre porositetsmodellering hade porositetsdata från flera borrhål varit att föredra.

Faciesmodellering genomfördes för en lagerföljd där fyra facies (bergartstyper) hade identifierats: lersten, siltsten, finkornig sandsten och medelkornig sandsten. Två typer av simuleringsalgoritmer användes, en algoritm av trunkerande Gaussisk typ (*gtsim*) och en sekventiell indikatorsimuleringsalgoritm (*sisim*).

Två typer av *gtsim* simuleringar gjordes, en med ett beräknat variogram i vertikal led och ett med ett standard variogram. Ett variogram beskriver variationen mellan två mätpunkter. Från ett variogram kan en så kallad nugget erhållas vilket är variationen mellan två mätpunkter som är lokaliserade väldigt nära varandra samt en så kallad range vilket är avståndet där sambandet mellan mätpunkterna upphör. Enligt SGU fanns det en ordningssekvens mellan de olika facierna med lersten följt av siltsten följt av finkornig sandsten följt av medelkornig sandsten. *Gtsim* tog hänsyn till detta villkor när standardvariogrammet användes med en längre range. Vid användandet av *sisim* kunde ett variogram för varje facie användas men nackdelen var att den naturliga sekvensen inte togs hänsyn till vilket resulterade i en orealistiskt geologisk modell.

1. INTRODUCTION AND OBJECTIVE	1
2. BACKGROUND	3
2.1. CARBON CAPTURE AND STORAGE	3
2.1.1. <i>Capture and transport</i>	3
2.1.2. <i>CO₂ Storage</i>	4
2.1.2.1. Trapping mechanisms	5
2.1.2.1.1. Physical trapping	5
2.1.2.1.2. Geochemical trapping	5
2.2. CCS IN SWEDEN	6
2.3. SOUTHWEST SCANIA SITE	7
2.3.1. <i>Arnager greensand</i>	7
2.3.2. <i>Höganäs formation</i>	8
2.3.4. <i>Cap rock</i>	8
3. PETREL	9
3.1. WELL LOGS	9
3.1.1. <i>Neutron log</i>	9
3.1.2. <i>Density log</i>	10
3.2. VARIOGRAMS	10
3.2.1. <i>Indicator variograms</i>	13
3.3. MODELING AND SIMULATION	13
3.3.1. <i>Algorithms</i>	14
3.3.1.1. The sequential Gaussian simulation algorithm	15
3.3.1.2. The truncated Gaussian simulation algorithm	16
3.3.1.3. The sequential indicator simulation algorithm	17
4. MODELING WITH APPLICATION TO SOUTH SCANIA DATA	19
4.1. OVERVIEW	19
4.2. DATA	19
4.3. CREATION OF SURFACES	19
4.4. CREATION OF HORIZONS AND ZONES	20
4.5. WELLS	21
4.6. CREATION OF FACIES	24
4.7. UPSCALING AND LAYERING	24
4.8. POROSITY DATA ANALYSIS	25
4.8.1. <i>Porosity data transformation</i>	25
4.8.2. <i>Porosity data variogram analysis</i>	26
4.9. FACIES DATA ANALYSIS	26
4.9.1. <i>Gtsim variogram analysis</i>	28
4.9.2. <i>Sisim variogram analysis</i>	29
5. RESULTS	30
5.1. POROSITY STATISTICS	30
5.1.1. <i>Porosity statistics alternative multilayered trap</i>	32
5.2. STOCHASTIC POROSITY SIMULATION FOR SECONDARY TRAP	33
5.3. STOCHASTIC FACIES SIMULATION-GTSIM	35
5.3.1. <i>Gtsim with computed vertical variogram</i>	36
5.3.2. <i>Gtsim with default vertical variogram</i>	37
5.4. STOCHASTIC FACIES SIMULATION-SISIM	39
5.5. VOLUME CALCULATION	39

6. DISCUSSION	41
6.1. POROSITY MODELING	41
6.2. TRUNCATED GAUSSIAN SIMULATION	42
6.3. SEQUENTIAL INDICATOR SIMULATION	42
6.4. VOLUME CALCULATION	42
7. REFERENCES	43
APPENDIX A	45
APPENDIX B	46
APPENDIX C	47
APPENDIX D	49
APPENDIX E	50

1. INTRODUCTION AND OBJECTIVE

From preindustrial time to the year of 2005 the global atmospheric CO₂ concentration increased from 280 ppm to 379 ppm (fig. 1). The reason for this increase in global atmospheric CO₂ concentration is most likely anthropogenic use of fossil fuels (IPCC¹, 2007). According to the IPCC (2007) it is very likely that the increased emission of CO₂ has had an impact on the global climate. Among many indications of climate change IPCC (2007) mentions that:

- Annual average arctic sea ice extent has decreased by 2.7 % per decade since 1978
- There is observational evidence of an increase in intense tropical cyclone activity in the North Atlantic
- Eleven of the last twelve years (1995–2006) rank among the 12 warmest years in the instrumental record of global surface temperature (since 1850).

If mitigation measures are not being taken to lower global CO₂ emission IPCC (2007) claims that the consequences of a continued global climate change may be severe. Carbon Capture and Storage (CCS) has been suggested as a way of lowering the global atmospheric emission of CO₂. Estimations of total global CO₂ storage capacity are uncertain but it is likely that there is a storage capacity of at least 2000 Gt CO₂ worldwide. To achieve stabilization of an atmospheric CO₂ concentration between 450 and 750 ppm², CCS could contribute by 15 to 55 % of the mitigation effort until 2100 (IPCC, 2005). Thus CCS singlehandedly will not provide sufficient global CO₂ emission reduction needed, but together with other methods for climate change mitigation sufficient emission reductions may be reached to achieve stabilization (IPCC, 2005).

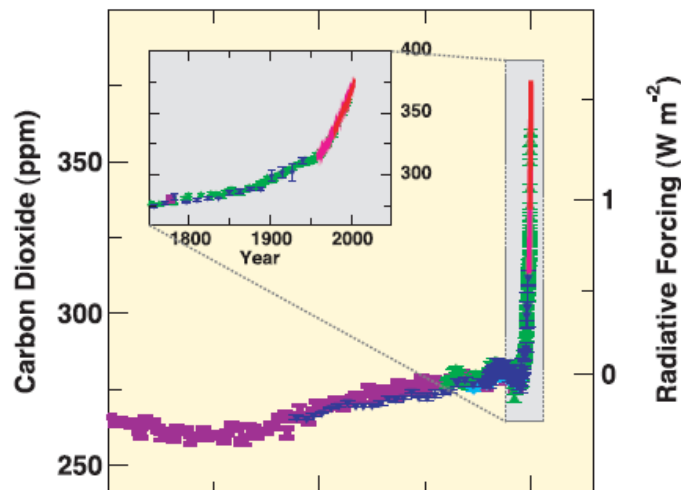


Figure 1. Change in atmospheric CO₂ content over time (IPCC, 2005).

The possibilities for CO₂ storage are limited in Sweden due to the bedrock type found here (Erlström, 2011). Most of the Swedish bedrock is very old, mainly originating from

¹ Intergovernmental Panel on Climate Change

² A rate often used in CO₂ stabilization scenarios (IPCC, 2005)

Precambrian time³ (SGU, 2010). This old Precambrian bedrock does not have the properties required for CO₂ storage such as sufficient permeability and porosity (Erlström, 2011). Younger⁴ sedimentary⁵ bedrock however may also be found on some locations and this is where saline aquifers suitable for CO₂ storage may be located (Erlström, 2011). One such location is the south Scania site where SGU in the realms of MUSTANG, a four year (2009-2013) large-scale integrating European project funded by the EU FP7 have been undertaking investigations regarding CO₂ sequestration possibilities.

The objective of the present Master thesis work was to construct a 3D site model in modeling/simulation software Petrel by using existing well log and geophysical data from the south Scania site. Special emphasis was in building the large scale 3D model evaluating geostatistical data as well as the stochastic simulation of the properties *porosity* and *facies*⁶ by using different geostatistical algorithms and evaluating the benefits in the use of each algorithm. The aim was to produce a 3D model to be used for CO₂ injection simulation purposes in the continuing work of MUSTANG.

³ More than 542 million years old

⁴ Youngest Swedish bedrock is about 55 million years old and can be found in Southwest Scania

⁵ Sedimentary rocks are formed on the earth's surface from sedimentation/deposition of weathering and erosion products from igneous, metamorphic or other sedimentary rocks

⁶ Facies is a term describing the characteristics of a rock that reflects its origin and is used to distinguish it from different rocks around it (Schlumberger, 2008)

2. BACKGROUND

2.1. CARBON CAPTURE AND STORAGE

Carbon Capture and Storage (CCS) has been suggested as a way of lowering the global atmospheric emission of CO₂. CCS consists of two steps: *Capture* and the actual *Storage* which may occur at various forms of locations. Focus in this report is on geological storage, injection of CO₂ into the bedrock.

2.1.1. Capture and transport

Carbon capture is the process in which the carbon is separated from the fossil fuel. The purpose is to produce a high pressure concentrated CO₂ stream that can be transported to a storage location (IPCC, 2005). There are mainly three different Carbon capture techniques: *post combustion capture*, *pre combustion capture* and *oxyfuel capture*.

Post combustion is the most widely used carbon capture technique. In this process the fossil fuel is combusted with air generating heat, energy and flue gas. The flue gas contains low amounts of CO₂ (4-14 %) so the CO₂ needs to be separated from the flue gas. Absorption and adsorption are the most common separation techniques (Pires, 2011).

The idea with the pre-combustion capture process is to remove the majority of the CO₂ from the fossil fuel before it is combusted. The fossil fuel is reformed into a gas mixture consisting mostly of CO and H₂O (Vattenfall, 2010a) but also small particles. The small particles are removed from the gas mixture and the carbon monoxide is thereafter reacted with water vapor, $CO + H_2O \leftrightarrow CO_2 + H_2$. The CO₂ is transported to the storage location and the H₂ is used as fuel (Vattenfall, 2010a).

The combustion in the oxyfuel capture process is done with pure oxygen. The flue gas from the combustion process is cleaned from particles (water, sulfur etc.) by a sequence of steps and the flue gas at this point mainly consists of water vapor and carbon dioxide (Vattenfall, 2010b). Combustion temperatures with pure oxygen however are very high, in a regular combustion process the nitrogen in the air acts as a cooler but with nitrogen absent, recycled cleaned flue gas is used instead as a temperature sink (Pires, 2011). The water vapor thereafter condensates when the cleaned flue gas is cooled down leading to an almost pure CO₂ stream (Vattenfall, 2010b).

When the CO₂ has been captured it needs to be transported to a storage location. The knowledge on CO₂ transport is quite good since CO₂ has been used and transported in the petroleum industry for a long time (DOE, 2011). The CO₂ may be transported by pipelines or, in rare cases, ships (IPCC, 2005).

2.1.2. CO₂ Storage

There are two types of CO₂ storage; ocean storage and geological storage. Possible storage formations⁷ for geological storage include depleted oil and gas fields, deep coal seams and saline aquifers (IPCC, 2005). Focus in this report will be on saline aquifers⁸.

The water in deep aquifers is saline due to high concentration of dissolved salts. At 1000 m the salinity is normally around 10 % (Erlström, 2011). This saline water is called brine. At a certain depth and temperature CO₂ becomes supercritical with liquid-like densities around 500-800 kg/m³, an advantageous characteristic for the storage efficiency. This is the reason why injections often are done at depths below 800 m. There are however exceptions.

Injections at The CO₂SINK pilot project at Ketzin, Germany are done at 625 m (Wurdemann, 2010). CO₂ has been injected into reservoirs⁹ for a long time to enhance oil recovery. It was first tried in 1972 in Scurry County, Texas (DOE, 2011). Knowledge on CO₂ injection into reservoirs therefore is good.

Deep saline aquifers are considered to be the formations with the highest potential capacity globally for CO₂ storage (Michael, 2010), around 1000 Gt CO₂ (IPCC, 2005). CO₂ injection into deep saline aquifers first took place in the 1990s in Canada (Michael, 2010). Today there are four commercial-scale CO₂ storage projects in saline aquifers: Alberta Basin, Canada which started in 1990, Sleipner, Norway (1996), Snøvit, Norway (2008) and In Salah, Algeria (2004) (Michael, 2010).

In a review of the experience on geological storage of CO₂ in saline aquifers from existing storage operations it could be seen that in the existing saline storage aquifers of today injection depth varied between 650 and 2800 m, average reservoir porosity also varied a great deal, between 5 and 35%. Most common was injection into siliciclastic¹⁰ aquifers; injection into carbonate¹¹ aquifers was rare (Michael, 2010). Injection strategies varied depending on the characteristics of the aquifers. In general high formation permeability enabled higher injection rate and the need of fewer wells (Michael, 2010).

When injecting CO₂ into a saline aquifer, there is a risk of leakage. A well chosen CO₂ storage location should not leak. There are however two different scenarios that might lead to leakage; one is abrupt leakage which is when there is leakage up an abandoned well or leakage due to injection well failure. The other is gradual leakage which is when there is leakage through undetected faults, fractures or wells (IPCC, 2005). Different monitoring activities are taking place to make sure leakage is not occurring at the existing storage locations (IPCC, 2005).

⁷ Geological unit composed by several layers of sedimentary rocks or soils that in some ways have similar properties

⁸ An underground layer of sedimentary rocks containing large amounts of water due to its permeable properties

⁹ Geological unit composed by a body of rock having sufficient porosity and permeability to transmit and store fluids

¹⁰ Siliciclastic means that its texture consists of discrete fragments and particles mainly from silicate minerals (minerals that have the silicon-oxygen tetrahedron as their basic structure) that are cemented and compacted together

¹¹ Made of carbonate minerals, minerals comprising of the carbonate ion CO₃²⁻

2.1.2.1. Trapping mechanisms

When the CO₂ has been injected into an aquifer it is trapped by different mechanisms depending on the time after injection (fig. 2). It can either be physically trapped, which is the initial trapping mechanism, or geochemically trapped, which is a much slower trapping mechanism.

2.1.2.1.1. Physical trapping

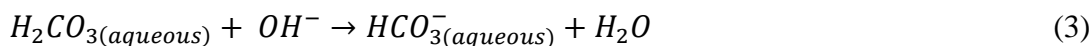
Adsorption trapping is one way of physical entrapment and occurs when the CO₂ adsorbs onto organic materials on coals and shales¹² in the formation. Stratigraphic and structural trapping occurs when the CO₂ is hindered from migrating upwards by a low permeable layer also called a cap rock. Typical cap rocks include shale, anhydrite¹³, salt (Schlumberger, 2008), clay, claystone or loamy limestone (Erlström, 2011). The term stratigraphic indicates that there are no faults or folds in the geometric subsurface, otherwise it is structural (CO₂CRC, 2011). Another form of physical trapping is residual trapping: When CO₂ migrates through the porous media in the aquifer some of the CO₂ is trapped along the way in pore spaces and made immobile (Bachu, 2007). Hydrodynamic trapping occurs when CO₂ displaces saline formation water. The less dense CO₂ migrates upwards to the top of the formation. The CO₂ then migrates as a separate phase until it is trapped in structural or stratigraphic traps or as residual CO₂. It may also be dissolved in the formation brine and follow the migration of the groundwater (IPCC, 2005).

2.1.2.1.2. Geochemical trapping

Solubility trapping is when CO₂ dissolves (eq. 1) and reacts with aquifer brine and forms dihydrogen carbonate (eq. 2) (Bachu, 2007). Roughly 20-60 kg of CO₂ can dissolve into 1 m³ aquifer brine depending on the pressure and salinity (Erlström, 2011). CO₂ solubility increases with increased pressure, but decreases with increased temperature and salinity (IPCC, 2005). 20-30 % of injected CO₂ may be dissolved into the aquifer brine over a period of 100 years (Erlström, 2011).



The geochemical trapping continues when hydrogen carbonate is formed in a process between the dihydrogen carbonate and the aquifer minerals (eq. 3) (Bachu, 2007). This trapping process dominates from hundreds to thousands of years and is called ionic trapping (IPCC, 2005)



Finally in a two step reaction a solid mineral is formed (eq. 4) and (eq. 5) (Bachu, 2007). Mineral trapping is the safest way of long-term CO₂ storing but is a very slow process

¹² Sedimentary rock mainly consisting of clay minerals

¹³ Mineral consisting of calcium sulfate, CaSO₄

dominating over a thousand to millions of years (IPCC, 2005). Minerals involved in the reaction are either carbonate or silicate minerals.

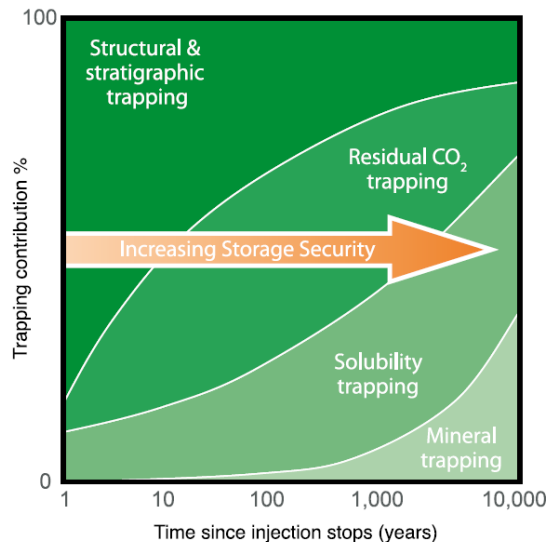
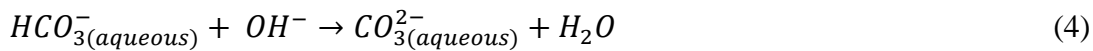


Figure 2. Trapping mechanisms and storage security over time (IPCC, 2005).

2.2. CCS IN SWEDEN

According to IEA (2010) CO₂ emissions in Sweden decreased from 52.8 Mt in 1990 to 45.9 Mt in 2008, thus a 13 % decrease. The Kyoto protocol target allowed Sweden to have a CO₂ emission increase of maximum 4 % by 2012 and this target will clearly be met.

Electricity in many parts of the world is produced by coal, gas or oil leading to great emissions of CO₂. The Swedish electricity production however is mostly generated by CO₂ emission neutral energy sources such as hydropower, nuclear power or bio fuel. The biggest source of CO₂ emissions in Sweden is from the heavy industry. In a mapping in 2008 it could be seen that the biggest CO₂ emission source in Sweden was steel company SSAB at two different locations; Luleå (3.4 Mt) and, Oxelösund (2.3 Mt) (Erlström, 2011). The paper production industry also stood for a large part of the Swedish CO₂ emissions. In the case of commercial carbon capture and storage in Sweden it would most likely be targeted towards Swedish industries and international industries in the close-by region.

Between 1970 and 1990 OPAB¹⁴ conducted seismic measurements at various locations around Sweden. These measurements are currently administered by SGU¹⁵. In the report “Lagring av koldioxid i berggrunden - krav, förutsättningar och möjligheter”¹⁶ (Erlström, 2011) evaluations of possible storage locations in Sweden were made mainly from the OPAB data. According to Erlström (2011) there are three locations of interest regarding CO₂ storage

¹⁴Oil Prospecting Corporation, affiliate to prospecting company Swedish Petroleum Exploration AB

¹⁵ Swedish Geological Survey

¹⁶ Storage of carbon dioxide in the bedrock- requirements, conditions and opportunities

in Sweden: Southern Baltic sea, Southern Kattegat and Southwest Scania. Focus in this report will be on the southwest Scania site.

2.3. SOUTHWEST SCANIA SITE

The area of interest in southwest Scania (fig. 3) forms a four km sedimentary bedrock multilayered sequence at its deepest locations. Initial drilling seems promising and the area appears to have the basic properties required for a CO₂ storage site with regards to depth, permeability, porosity etc. The area however shows great heterogeneity and lateral variation (Erlström, 2011). Deep drilling has been done at FFC-1 (fig. 3). An intersection of the area at FFC-1 can be seen in appendix A. There are two formations in the 3D site model area that might be suitable for CO₂ storage: Arnager greensand and the Höganäs formation. These formations are not limited only to the 3D site model area but stretch beyond.

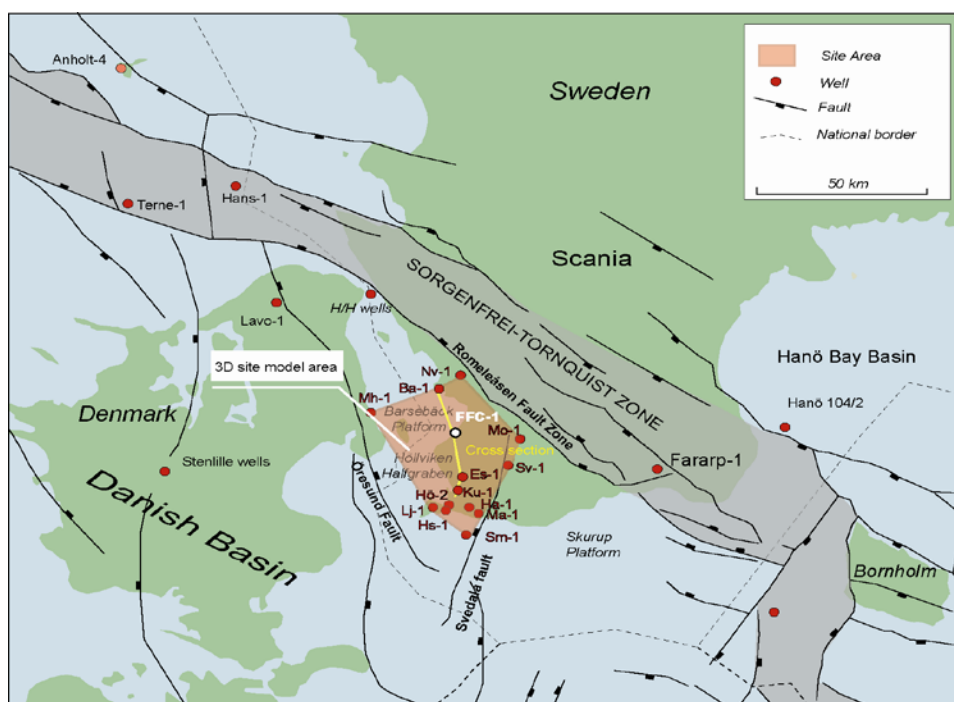


Figure 3. Mapping of south Sweden and the 3D site model area (Erlström, 2011, with permission).

2.3.1. Arnager greensand

The Arnager greensand covers a vast area. According to Erlström (2011) it is 20-60 m thick and relatively homogenous. The secondary trap and the primary trap belong to the Arnager greensand formation (appendix A). The storage properties of the Arnager greensand aquifer vary considerably. Permeability can vary as much as 900 mD between different locations. Beneath the Arnager greensand a thick interval of claystone originating from the lower cretaceous period with varying thickness can be found (Erlström, 2011). Among this claystone layer a sandstone¹⁷ layer with similar properties as the Arnager greensand also exists. The lateral spread and thickness of this layer is uncertain (Erlström, 2011). Another sandstone sequence follows where 1-3 highly permeable sandstone aquifers 10-20 m thick

¹⁷ A sedimentary rock is given the term sandstone when the majority of the grains are sand sized (0.063- 2.0 mm)

have been identified. This sequence covers a large area. It has not been dated but originates somewhere between lower cretaceous and lower jurassic (Erlström, 2011).

2.3.2. Höganäs formation

The Höganäs formation consists of sandstone aquifers in a multilayered sequence of siltstone, claystone and coal (Erlström, 2011). The alternative multilayered trap and the alternative trap belong to the Höganäs formation (appendix A). The formation is 150-250 m thick and comprises of 40-70 % of sandstone. The sandstone aquifers are scattered in the formation with a local expansion of some 10 km² and maximum thickness of around 20 m. The physical properties of these sandstone aquifers vary greatly. In the lower parts of the formation sandstone aquifer expansion appears to be larger (Erlström, 2011). The majority of the aquifers in the Höganäs formation consist of fine grained pure quartz sand. Porosity in these aquifers is quite high but nevertheless have a low permeability, often lower than 100 mD. However 10 % of the aquifers consists of medium or coarse grained sand and these aquifers are very permeable >1 D (Erlström, 2011).

2.3.4. Cap rock

A very thick layer sequence of different minerals such as limestone and claystone is located above these aquifers. This layer sequence appears to be very dense and would therefore act as a cap rock; however the properties of the cap rock have not been determined which makes it uncertain. There are also layer sequences of claystone as mentioned between the aquifers that could act as secondary seals (Erlström, 2011).

3. PETREL

Petrel (Schlumberger, 2010) (fig. 4) is a software for 3D visualization, 3D reservoir modeling and 3D mapping of the geological subsurface produced by oil/gas company Schlumberger. Petrel enables use of different modeling techniques (stochastic and deterministic) including facies modeling and various simulation algorithms as well as geostatistical tools and data transformations. By using various forms of geophysical and borehole data a geological subsurface of interest can be modeled and interpreted. Drilling and other ways of data gathering is often expensive and limited. Geophysicists, geologists and engineers thus rely to a great extent on software such as Petrel and the geostatistical algorithms implemented to model the area in question when data is scarce.

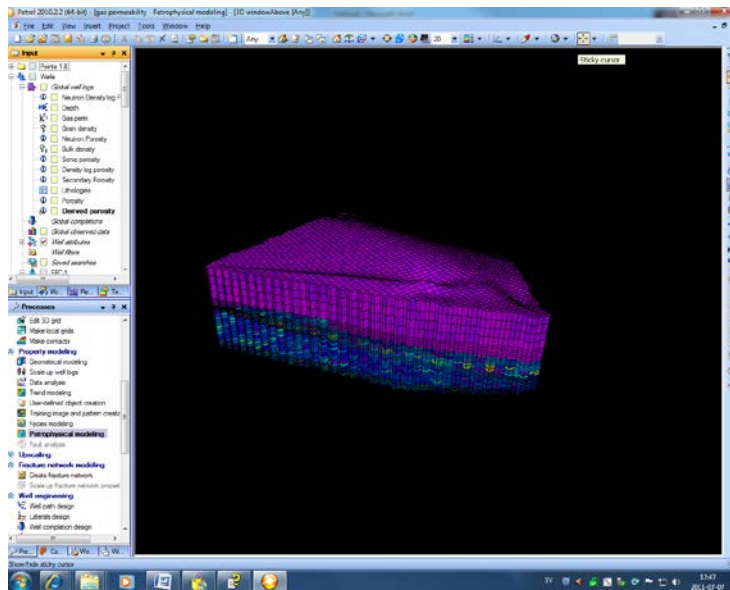


Figure 4. Petrel interface.

A geological 3D model is a visualization of a geological subsurface. The model is divided into boxes making up the 3D grid. These boxes/grid cells are given properties such as porosity and permeability, each grid cell will be given a single value of each property. Thus a high resolution grid with many grid cells is more sensitive for details and smaller variation but may lead to lengthy computation times.

3.1. WELL LOGS

Information on properties such as porosity and permeability are usually extracted from well logs. Well logs also called borehole logs are records of the geological subsurface penetrated by a drill. Information from the borehole can be extracted either by analyzing a sample from the borehole or by lowering instruments down into the borehole and making various measurements. Two kinds of well logs will be mentioned here: the neutron log and the density log, both logs being used to get an estimation of the porosity.

3.1.1. Neutron log

A neutron log responds primarily to the amount of hydrogen (H_2O or hydrocarbons) in a formation (Lyons, 2005). The neutron log is made from measurements of either gamma ray

particles or neutrons, both processes consisting of neutrons being emitted into the formation by a neutron source. When the neutron is being emitted into the formation it will start colliding with particles in the formation matrix, every collision will lower the energy of the neutron. The energy decrease is determined by the mass of the particle the neutron collides with (Lyons, 2005). A collision with a heavy particle will not have a great impact on the energy loss of the neutron but a collision with a particle of roughly the equal mass such as a hydrogen atom will. Thus neutrons being emitted into a formation containing substantial amounts of water will be slowed down fast. The neutrons being emitted from the source have energy levels of 4 MeV or greater. When the neutrons have decreased to an energy level of around 0.025 eV their final energy state has been reached and they will then diffuse randomly in the formation matrix until they are captured by the nuclei of atoms such as hydrogen or chlorine (Schlumberger, 1991) The nuclei of the capturing atom will emit a gamma ray particle. The neutron log equipment setup can either count these gamma ray particles or neutrons at different energy levels (Lyons, 2005) and from this get an estimation of the porosity.

3.1.2. Density log

A density log is made from measurements of gamma ray particles (Lyons, 2005). A radioactive source is attached to the borehole wall with one side shielded to avoid influence from parts of the formation not exposed by gamma ray particles from the radioactive source. In the formation the gamma ray particles from the radioactive source will collide with electrons and loose energy, this is called Compton scattering (Lyons, 2005). The amount of electrons and collisions with gamma ray particles is directly related to the electron density, meaning the higher electron density the more the gamma ray particles will collide with the electrons and scatter onto the detector. The relation between electron density and bulk density can be expressed $e_e = e_b \left(\frac{2Z}{A} \right)$ where e_e is the electron density, e_b the bulk density if the formation matrix consists of a single substance, z the atomic number of the formation material and A the atomic weight (Schlumberger, 1991).

3.2. VARIOGRAMS

A variogram is a measure of spatial variability in a certain direction for a random field where the spatial variability is expressed by the variance. The variogram is mathematically defined as (Bachmaier, 2008):

$$\gamma(\vec{h}) = \frac{1}{2} E \left[[Z(\vec{x} + \vec{h}) - Z(\vec{x})]^2 \right] = \frac{1}{2} Var[Z(\vec{x} + \vec{h}) - Z(\vec{x})] \quad (6)$$

where:

$\gamma(\vec{h}) = \text{theoretical variogram}$

$Z(\vec{x} + \vec{h}), Z(\vec{x}) = \text{random variables}$

$\vec{x} = \text{position vector}$

$\vec{h} = \text{distance between two points (the lag)}$

$E = \text{expected value}$

The principle of the variogram is that two closely located samples have less dissimilarity than two samples far away from each other. Beyond a certain distance called the range (fig. 5) dissimilarity is at its maximum. The nugget (fig. 5) is the variance when the distance between two measured samples is very close to zero. The separation distances between the search points are called lags. The directions (in Petrel) are labeled major, minor and vertical. The major direction is specified where dissimilarity is at a minimum and the minor direction is automatically perpendicular to the major direction. Consequently the major and minor ranges are given from the major and minor direction. The vertical range is given from the variogram computed in the vertical direction. The sill (fig. 5) is the variance when the variogram levels out.

The terms semivariogram/variogram and semivariance/variance are often used synonymously in geostatistical literature. According to Bachmaier (2008) the terms semivariance and semivariogram should not be used. The confusion stems from one early article on variogram analysis where the "variance of differences": $Var[Z(\vec{x} + \vec{h}) - Z(\vec{x})]$ was discussed.

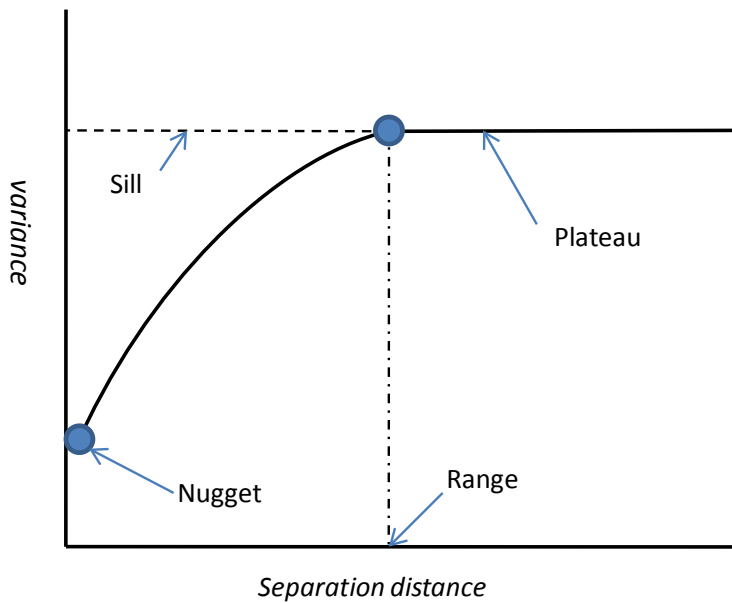


Figure 5. Example of a theoretical variogram.

In determining the theoretical variogram a sample variogram must first be plotted which is a cross plot between the dissimilarities of a specified location X_1 and each of several other points (X_2, X_3, \dots, X_n) with an increasing distance. For every pair $(X_1, X_2), (X_1, X_3), \dots, (X_1, X_n)$ the empirical variance (s^2) is plotted against their separation distance and can be expressed by (Bachmaier, 2008):

$$s^2 = \frac{1}{n-1} \sum_{i=1}^n (z_i - \bar{z})^2 \quad (7)$$

where the measured values are denoted by z_i and \bar{z} is the mean of the two values. When the sample variogram has been plotted a theoretical variogram is fitted to it. There are various equations for this estimation procedure with the following three variogram model options available in Petrel (fig. 6) (Schlumberger, 2010):

$$\text{Exponential} \quad \gamma(\vec{h}) = c \left[1 - \exp\left(-\frac{3\vec{h}}{a}\right) \right] \quad (8)$$

$$\text{Spherical} \quad \gamma(\vec{h}) = c \left[\frac{3\vec{h}}{2a} - \frac{1}{2} \frac{\vec{h}^3}{a^3} \right], \quad 0 \leq h \leq a \quad (9)$$

$$\gamma(\vec{h}) = c, \quad \vec{h} > a \quad (10)$$

$$\text{Gaussian} \quad \gamma(\vec{h}) = c \left[1 - \exp\left(-\frac{3\vec{h}^2}{a^2}\right) \right] \quad (11)$$

Where:

$c = \text{sill} - \text{nugget}$

$\vec{h} = \text{spatial vector, distance from central point}$

$a = \text{effective range (the distance where } \vec{h} \text{ equals 95\% of the sill)}^{18}$

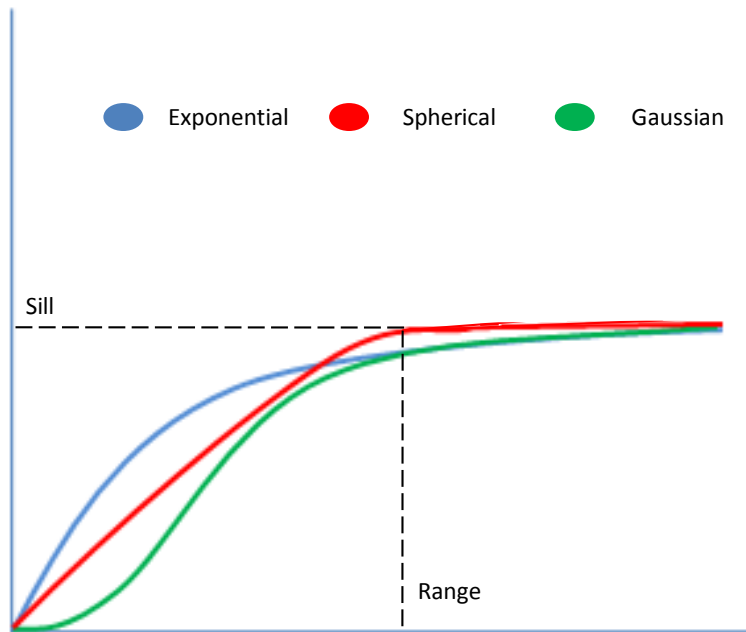


Figure 6. The three theoretical variogram model types available in Petrel.

The variograms and variogram parameters generated in Petrel are normalized to a sill of 1. The impact of the variogram parameters on a stochastic model can be seen in figure 7 where the spatial distribution of porosity in the model domain using porosity data from the FFC-1 well log in the modeling process varying the range and the nugget can be seen. A large range

¹⁸ For the spherical model effective range equals actual range

results (fig. 7 a) in less heterogeneity than a small range (fig. 7 b). However a large nugget value will override the effect of the range and lead to heterogeneous results even though the range is large (fig. 7 c).

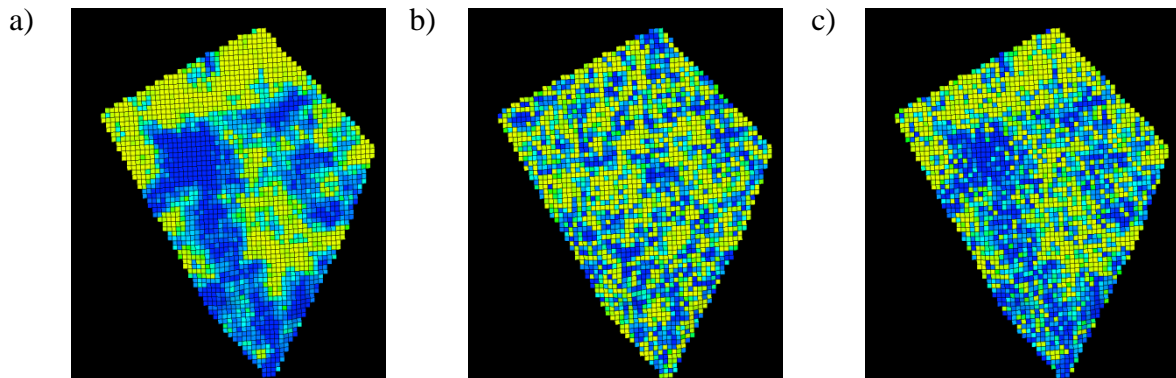


Figure 7. Porosity distribution generated in Petrel, stochastic model with a major and minor range of: a) 20 000 m and a nugget of 0. b) 2000 m and a nugget of 0. c) 20 000 m and nugget of 0.5.

3.2.1. Indicator variograms

Indicator variogram is the term for a variogram computed from discrete data. The variogram is determined for each facies separately. The value of "1" is given for the facies being calculated and the rest of the facies are given the value "0" (fig. 8). The rest of the computation process being the same as computing a "normal" variogram. These steps are repeated for each facies.

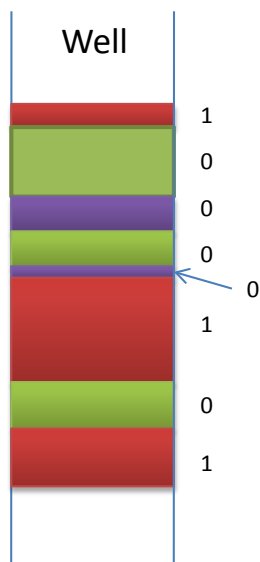


Figure 8. An example of how an indicator variogram is computed.

3.3. MODELING AND SIMULATION

"A simulation is a system of models having a definite resemblance to the first system (the original)" (Vann, 2002) where as a model is a measure or an image used to represent the spatial distribution of variables.

Two different modeling methods are available in Petrel, deterministic and stochastic modeling. A deterministic model is a model where no randomness is involved in the modeling process, thus the same result will be generated for every modeling run with the same input data. An example of a deterministic model run can be seen in figure 9 (a). A deterministic modeling algorithm will produce the same realization¹⁹ every time, which is "the best estimate". The deterministic approach requires great knowledge on the behavior of the variable being modeled. However very few earth science processes are understood in such detail. A stochastic approach is therefore more common.

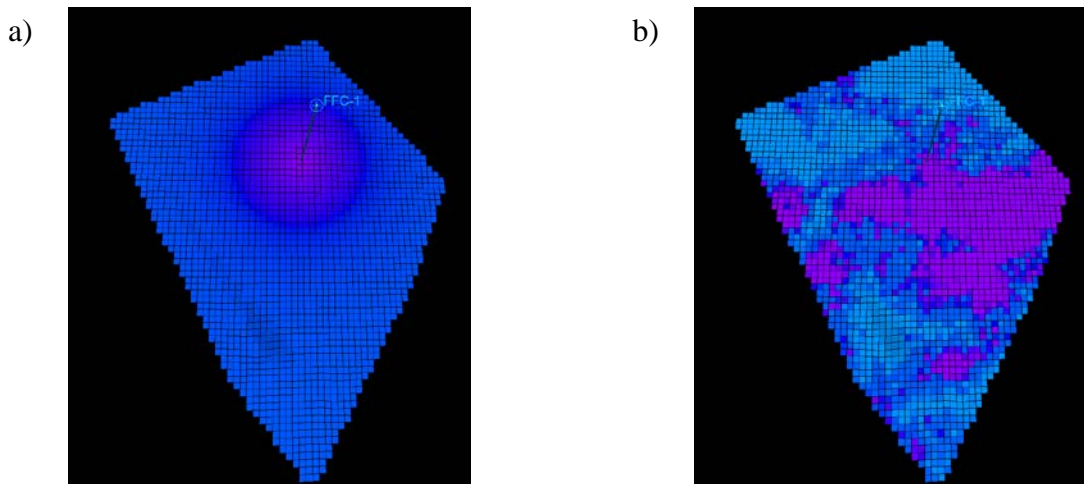


Figure 9. Porosity distribution generated in Petrel, location of FFC-1 and: a) example of a deterministic model. b) example of a realization of a stochastic modeling algorithm.

A stochastic simulation model is based on a series of realizations representing a range of possibilities. The range of these possibilities depending on the variogram, variance of the input data etc. These realizations will have similar outputs (with the same input data) but with varying details. Stochastic modeling algorithms are more complex than deterministic algorithms implementing randomness. The distribution of a stochastically modeled property will have a distribution more typical of the real case. The specific variations and locations however are unlikely to match. The same input data was used generating figure 9 (a) and (b). These figures show the spatial distribution of porosity in the model domain using porosity data from the FFC-1 well log in the modeling process using a deterministic and a stochastic modeling algorithm.

3.3.1. Algorithms

An algorithm is a set of instructions designed to solve a problem or carrying out a procedure. Three GSLIB²⁰ modeling algorithms implemented in Petrel were used in the modeling process: the sequential Gaussian simulation algorithm (*sgsim*), the truncated Gaussian simulation algorithm (*gtsim*), and the sequential indicator simulation algorithm (*sisim*). *Gtsim* however is not a modeling algorithm since it does not generate realizations but must be used

¹⁹ A quantitative description

²⁰ GSLIB(Geostatistical Software Library), one of the most widely used geostatistical software is an open source code developed at Stanford university (Deutsch, 1998)

in conjunction with *sgsim* for the purpose of modeling discrete data such as facies. *Sgsim* in its own is used for modeling of continuous data such as porosity. An interpretation of the *sgsim* and *gtsim* processes and the connections between them used in this study can be seen in figure 10. *Sisim* may be used for modeling of both continuous and discrete data.

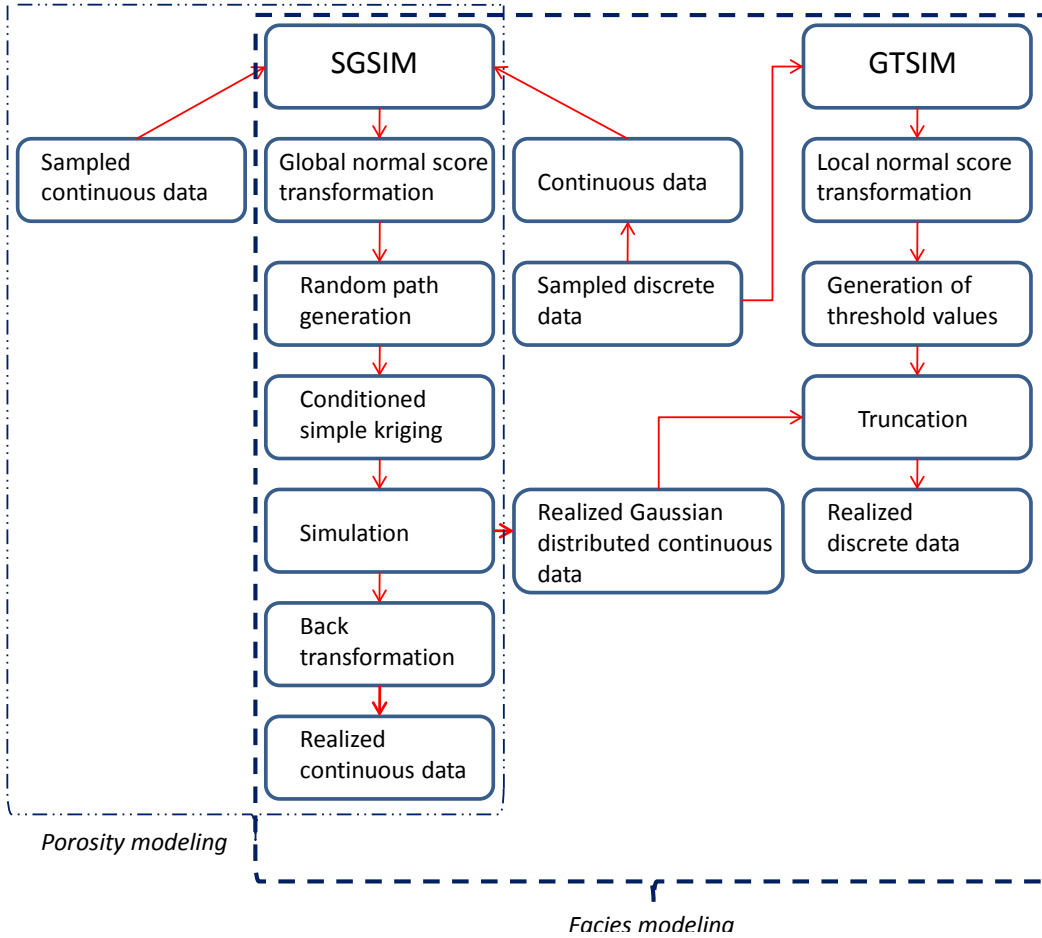


Figure 10. Overview of the interpretation of the *sgsim* and *gtsim* processes.

3.3.1.1. The sequential Gaussian simulation algorithm

The *sgsim* algorithm process consisted of the following steps (Deutsch, 1998):

The $cdf^{21} F_z(z)$ was determined for the entire area (the secondary trap) and was expressed as

$$F_z(z) = Prob\{Z_i \leq z_i, i = 1, \dots, N\} \quad (12)$$

N being the number of samples and the right hand side representing the probability that the random variable Z takes on a value less than or equal z . To ensure a standardized Gaussian distribution with a mean $\mu = 0$ and standard deviation $\sigma = 1$ the $cdf F_z(z)$ was normal score transformed into a standard normal $cdf F_y(y)$. Next, the variogram $\gamma(\vec{h})$ of the normal score transformed data was calculated. A random path visiting each grid node u was thereafter generated. The mean μ and variance σ^2 was sequentially estimated by simple kriging at each grid node u according to the random path being generated. The model parameters of the

²¹ Cumulative density function, in some geostatistical literature called cumulative distribution function, e.g. Deutch (1998)

normal score variogram, original data as well as previously simulated grid node values were used in the simple kriging (*SK*) process. Kriging is essentially the interpolation of a value $Z(u)$ from observations of values at close by locations $Z(u_\alpha)$ (fig. 11). This was done by solving a set of equations giving the best estimation to fit the points on the theoretical variograms overlapping it.

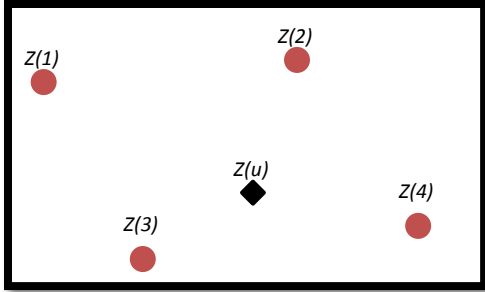


Figure 11. Unknown value at location u , known values at location 1-4.

The basic form of kriging can be expressed as:

$$[Z^*(u) - m(u)] = \sum_{\alpha=1}^n \lambda_{\alpha}(u)[Z(u_{\alpha}) - m(u_{\alpha})] \quad (13)$$

where

$Z^*(u)$ = linear regression estimator

u, u_{α} = estimation point and neighboring data point

$m(u), m(u_{\alpha})$ = expected values (means) of $Z(u)$ and $Z(u_{\alpha})$

$\lambda_{\alpha}(u)$ = kriging weight

The *SK* algorithm uses the global mean instead of using a local mean as is the case when using for example the ordinary kriging algorithm. Thus (eq. 13) could therefore be simplified into (eq. 14) since a constant and known mean was used $m(u) = m(u_{\alpha}) = m$.

$$Z_{SK}^*(u) = m + \sum_{\alpha=1}^n \lambda_{\alpha}(u)[Z(u_{\alpha}) - m] \quad (14)$$

By using the estimated mean μ and variance σ^2 , a local *cdf* at each grid node u was generated. A simulated value $y^{(l)}(u)$ was then randomly drawn from that *cdf*. This was carried out for each grid node u until all grid nodes had been visited.

The simulated normal values $\{y^{(l)}(u), u \in A\}$ were finally back transformed into the original variables according to the original distribution $\{z^{(l)}(u) = \varphi^{-1}(y^{(l)}(u)), u \in A\}$.

3.3.1.2. The truncated Gaussian simulation algorithm

The *gtsim* algorithm consisted of the following steps (Journel, 2001):

The local *cdf* ($F(u; s_k)$) was determined at each grid node u :

$$F(u; s_k) = Prob\{S(u) \leq s_k\} \forall k = 1, \dots, K \quad (15)$$

where $S(u)$ is a variable classified into a certain number of classes $S(u) \in \{s_k, k = 1, \dots, K\}$ and s_k is a numerical code assigned to the k th class.

Each local *cdf* was then normal score transformed into a Gaussian distributed *cdf*. Normal score threshold values $t(u; s_k)$ (fig. 12) were determined from the local *cdf*'s $F(u; s_k)$ by the quantile transform:

$$t(u; s_k) = \begin{cases} -\infty & k = 0 \\ G^{-1}(F(u; s_k)) \in (-\infty, +\infty] & k = 1, \dots, K \end{cases} \quad (16)$$

where $G^{-1}(\cdot)$ is the standard normal quantile function.

Realizations $y^{(l)}(u)$ were generated by *sgsim*. The realizations in *sgsim* were based on the original discrete sample data $s(u_\alpha)$, *sgsim* however being a simulation for continuous data requiring a transformation from discrete to continuous form for $s(u_\alpha)$. The realizations $y^{(l)}(u)$ were then truncated with the generated threshold values $t(u; s_k)$ for the generation of discrete data $s^{(l)}(u)$ (fig. 12).

$$s^{(l)}(u) = s_k \text{ if } y^{(l)}(u) \in (t(u; s_{k-1}), t(u; s_k)] \quad (17)$$

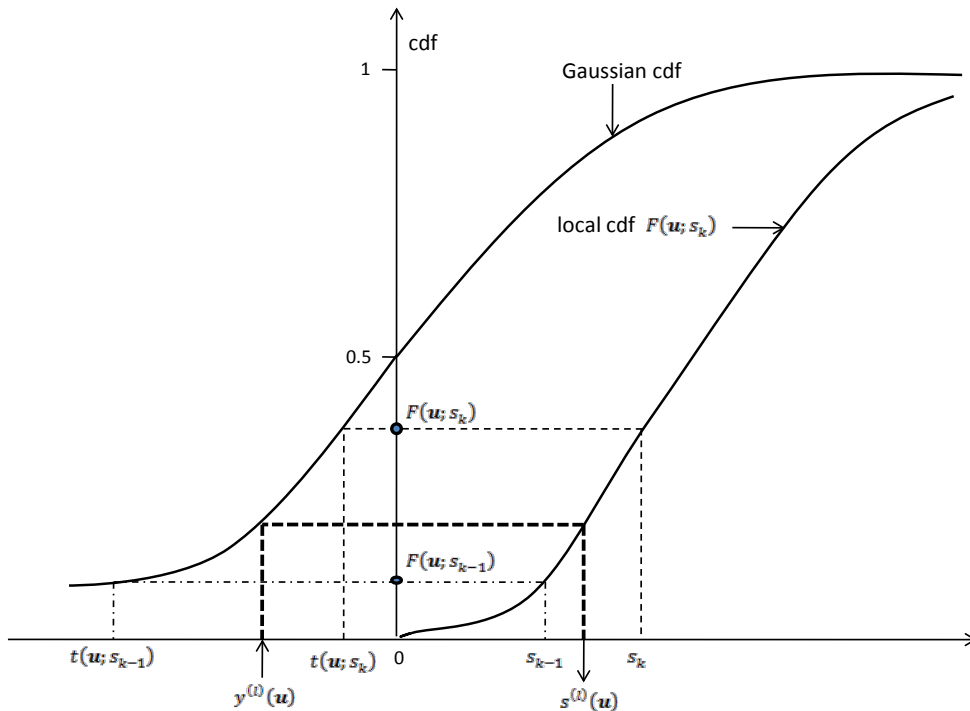


Figure 12. Connections between a local *cdf* and a normal scored transformed Gaussian *cdf* (after Journel, 2001).

3.3.1.3. The sequential indicator simulation algorithm

The sequential indicator simulation (*sisim*) and the *sgsim* both being sequential simulation algorithms have a similar algorithm process.

Consider K different categories s_k , $k = 1, \dots, K$ where $i(u; s_k) = 1$ if category s_k prevails at location u , 0 otherwise. A random path was determined visiting each grid node u where a *cdf* was determined for each category $k = 1, \dots, K$ by indicator kriging. Indicator kriging of the indicator variable $i(u; s_k)$ estimated the probability that s_k prevailed at location u (Deutch, 2008):

$$Prob^*\{I(u; s_k) = 1|(n)\} = p_k + \sum_{\alpha=1}^n \lambda_{\alpha} [I(u_{\alpha}; s_k) - p_k] \quad (18)$$

where

$I(u; s_k)$ = indicator random function at location u and for category s_k

p_k = stationary mean of the indicator of category k

λ_{α} = kriging weight

$*(n)$ = conditioning to n other neighboring variables

A random ordering of the K probabilities was thereafter set and one *cdf* was generated from the K *cdfs*. A random number p uniformly distributed in the interval $[0,1]$ was randomly generated. The interval where that number p fell resulted in the simulated category at location u (fig. 13).

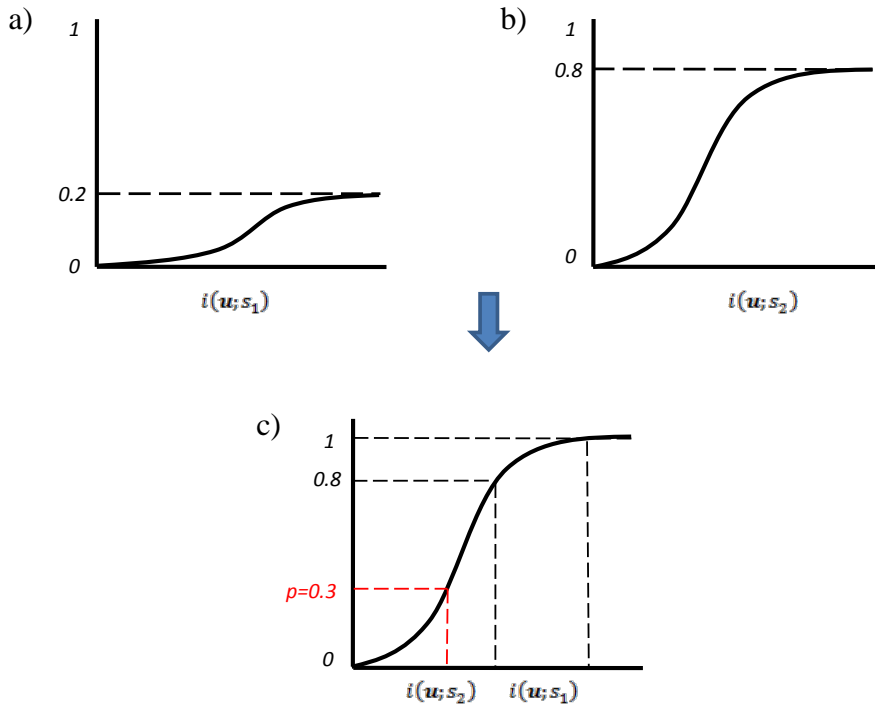


Figure 13. a) *cdf* of $i(u; s_1) = 1$. b) *cdf* of $i(u; s_2) = 1$. c) combined *cdf* of $i(u; s_1)$ and $i(u; s_2)$ and the random generated number $p = 0.3$.

4. MODELING WITH APPLICATION TO SOUTH SCANIA DATA

4.1. OVERVIEW

Constructing a 3D model in Petrel consists of many steps depending on what data is given. An overview of the process in this study is given in figure 14 and the steps will be explained in the following sections. The first six steps were carried out for all zones. Facies data analysis and facies modeling was carried out for the alternative multilayered trap (appendix A) belonging to the Höganäs formation. Porosity modeling was carried out for the secondary trap (appendix A), also referred to as the Arnager greensand aquifer.

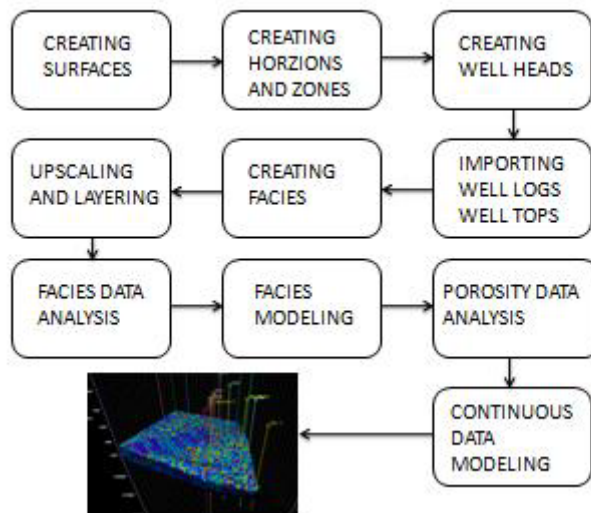


Figure 14. Overview of the modeling process in this study.

4.2. DATA

The data used to create the 3D model was received from SGU and consisted of 8 ASCII²² files with coordinates in XYZ format describing the surfaces, 1 well log file containing porosity information and an excel sheet with depth information of the surfaces as well as location of the wells. The data can be seen in appendix B.

4.3. CREATION OF SURFACES

First step in construction of the 3D model was to convert the XYZ points into surfaces. A convergent interpolation algorithm in the "Make/edit surface" process was used. The convergent interpolation algorithm is an iterative algorithm which converges on the solution (a final surface) by each iteration. Every iteration in the convergent interpolation algorithm consisted of three steps:

1. Refine -Increase of grid resolution
2. Snap -Re gridding of the data
3. Smooth -Minimizing curving of the grid

The resulting model for surface 1 (Top Granvik Member) beneath the XYZ points after convergent interpolation can be seen in figure 15 (a).

²² American Standard Code for Information Interchange

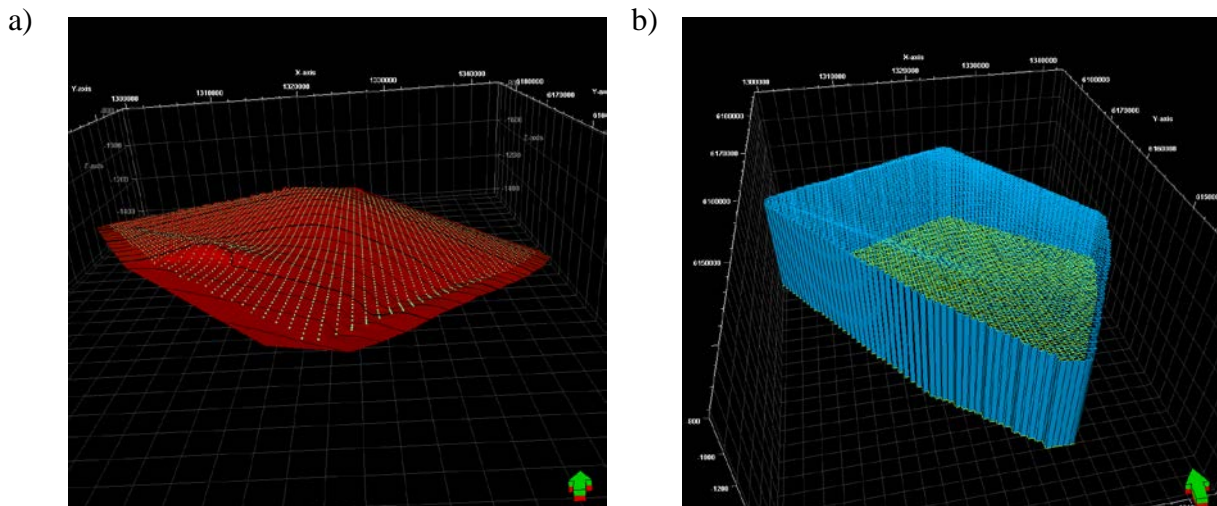


Figure 15. Grid and surface generated in Petrel using data provided by SGU. a) XYZ points and its subsequent surface. b) Primary grid.

Since no data on faulting was received the "Make simple grid" process was used providing a simpler alternative than the "Pillar gridding" process used for faulted geological sub surfaces. Surface 1 was set as top surface and surface 8 was set as bottom surface. The grid size and position were automatically set from the input data (surface 1 and 8) and the grid increment was set to $Xinc=750$ m and $Yinc=750$ m. The resulting grid can be seen in figure 15 (b).

4.4. CREATION OF HORIZONS AND ZONES

For the surfaces to be incorporated into the 3D grid they needed to be transformed into horizons which was done in the "Make horizons" process. With the creation of the eight horizons, seven zones were created automatically in between the horizons (fig. 16). The zones, in turn, were divided into layers at a later stage.

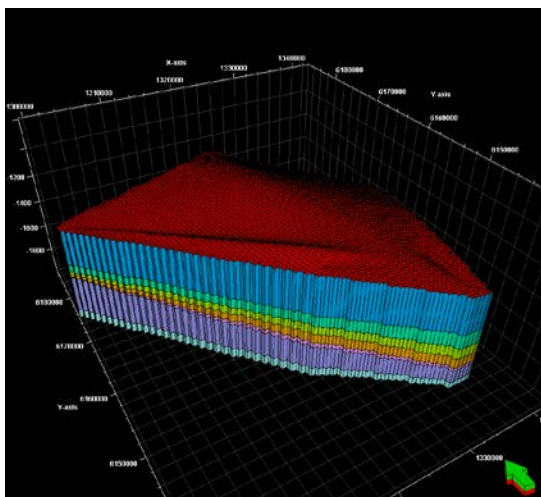


Figure 16. Model horizons and zones generated in Petrel using data provided by SGU.

4.5. WELLS

When working with wells in Petrel the existence of a well head is needed. A well head is simply information on the well such as its location, name and depth. Well heads can be created interactively in Petrel as well as being imported. No well heads files were given and thus the well heads were created in Petrel setting X, Y, KB²³ and TVD²⁴ given from the SGU data.

The FFC-1 well log contained porosity data determined by neutron and sonic measurements (appendix C) and bulk density determined by gamma ray particles measurements. The imported neutron log porosity (φ_n) for FFC-1 can be seen in figure 17 (a). The imported bulk density log for FFC-1 can be seen in figure 17 (b). The bulk density (ρ_B) was transformed into a density log porosity (fig. 17 b) by: $\varphi_d = \frac{(\rho_B - \rho_{ma})}{(\rho_f - \rho_{ma})}$ (Lyons, 2005), where ρ_{ma} is the matrix density and ρ_f the fluid density. The matrix density ρ_{ma} was set to 2.65 g/cm³ which is common for a sandstone formation with a porosity larger than 10% (Schlumberger, 1991) and the fluid density to 1.116 g/cm³ given from the R1 Arnager Greensand characterization (Erlström, personal communication).

²³ Kelly Bushing value, the altitude above sea level of the drill.

²⁴ True vertical depth from Kb

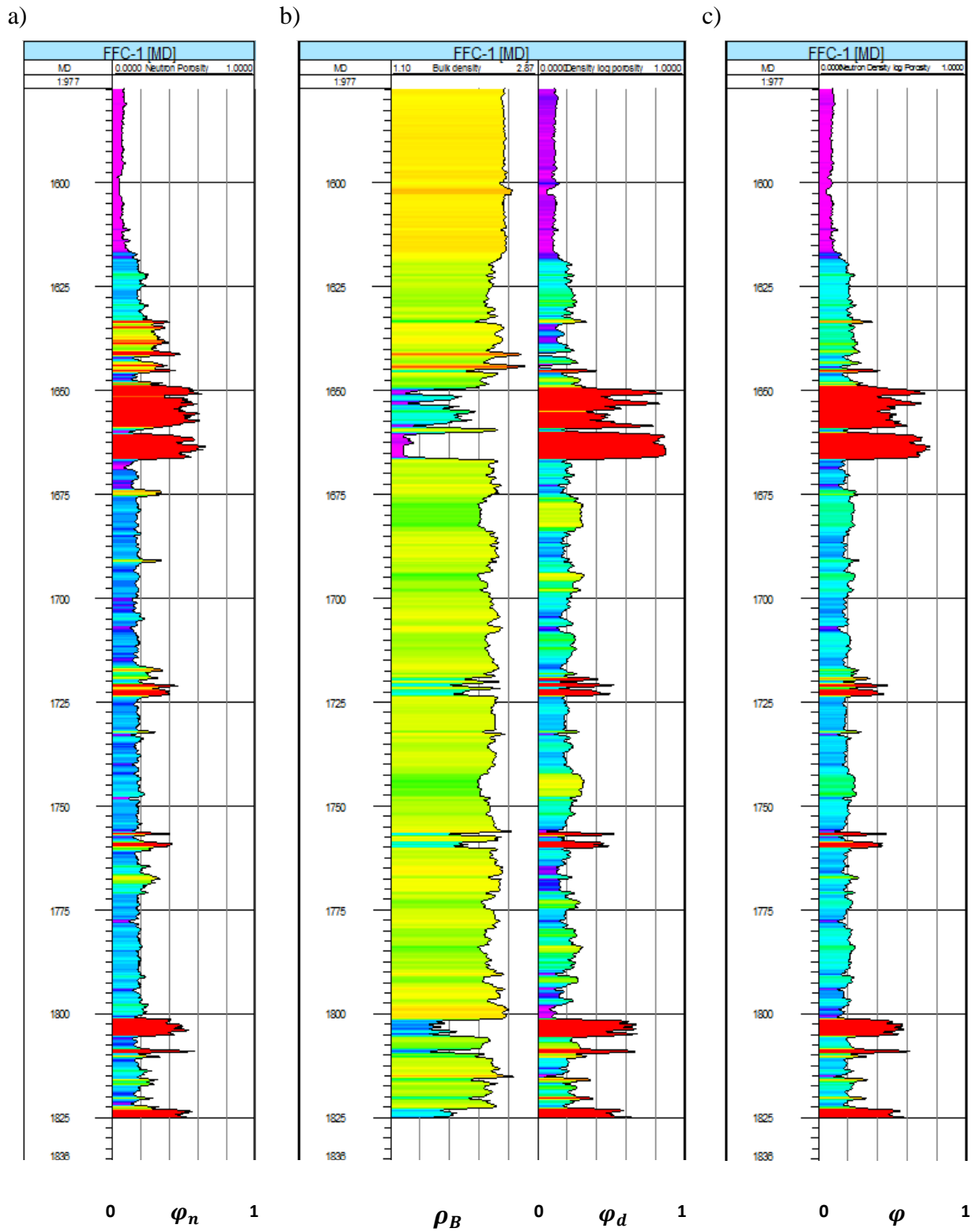


Figure 17. Well logs generated in Petrel using data provided by SGU. a) FFC-1 neutron log. b) FFC-1 bulk density log. c) Combined density log/neutron porosity in FFC-1 well section.

It is possible to estimate the porosity of a formation from a single "porosity log"²⁵, however a combination of porosity logs usually gives better results. The most common combination is the neutron-density log combination. To determine the porosity (φ_d) from the bulk density log (ρ_B) a value of 2.65 g/cm³ was used, this value however only gives accurate porosities for the matrix where sandstone is in fact dominating. If Limestone²⁶ or other minerals dominate in the particular formation matrix then the porosity computed from the bulk density log will not be accurate. However when the porosity from the neutron log and the porosity computed from the bulk density log are averaged (fig. 17 c) the lithology effects are to a great extent canceled out and a porosity very close to the true porosity is given (Dewan, 1983). Averaging was done by an arithmetic mean, $\varphi = \frac{\varphi_d + \varphi_n}{2}$ in the "global well logs calculator".

With the well logs in place the well tops were imported. Well tops are intersection points between structural surfaces and boreholes and are used as a control when modeling the positions of the horizons. Figure 18 (a) shows a section of the FFC 1-well before application of well tops. It could be seen that the horizons and the well tops were not identically located. After applying the well tops in the "Make horizons" process the horizons and well tops merged (fig. 18 b). The combined density log/neutron porosity φ in the FFC-1 well section with the integrated horizons can be seen in appendix D.

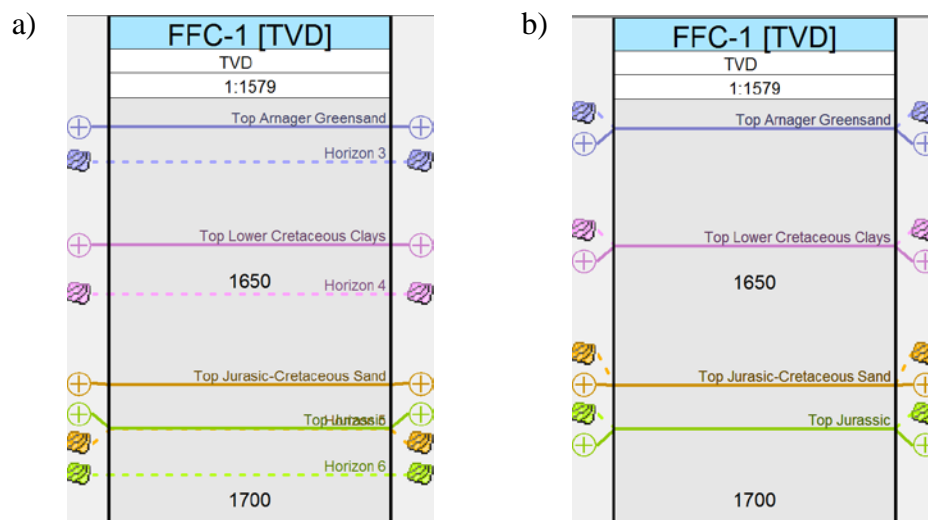


Figure 18. Model horizons and well tops generated in Petrel using data provided by SGU. a) FFC-1 well section with horizons and well tops. b) FFC-1 well section with integrated horizons and well tops.

²⁵ Neutron, density or sonic log

²⁶ 2.71 g/cm³

4.6. CREATION OF FACIES

In Petrel facies is regarded as a discrete property and is represented by an integer value. Facies modeling was done for the alternative multilayered trap where four different types of facies existed. The facies were constructed manually in Petrel (fig. 19 b) on the basis of the FFC-1 composite log (fig. 23). The facies were constructed with the "create new discrete log" tool available in the well section.

4.7. UPSCALING AND LAYERING

Upscaling was done to upscale the log data to the cells being penetrated by the FFC-1 well. Each cell being penetrated by the well was given a single value of the property in question. After the cells being penetrated by the wells had been detected the log data falling into the cells were averaged depending on which averaging algorithm that was chosen. The arithmetic mean algorithm, $\varphi_A = \frac{1}{N} \sum_{i=1}^N \varphi_i$, was used for the porosity upscaling (fig. 19 a). The averaging algorithm "most of" was used when the lithology facies log was upscaled (fig. 19 b). The "Most of" algorithm upscales the value being most represented in the penetrated cell.

Layering is the process when a zone is subdivided into internal layers, the layering is manually carried out to accurately depict the original log (fig. 19 a).

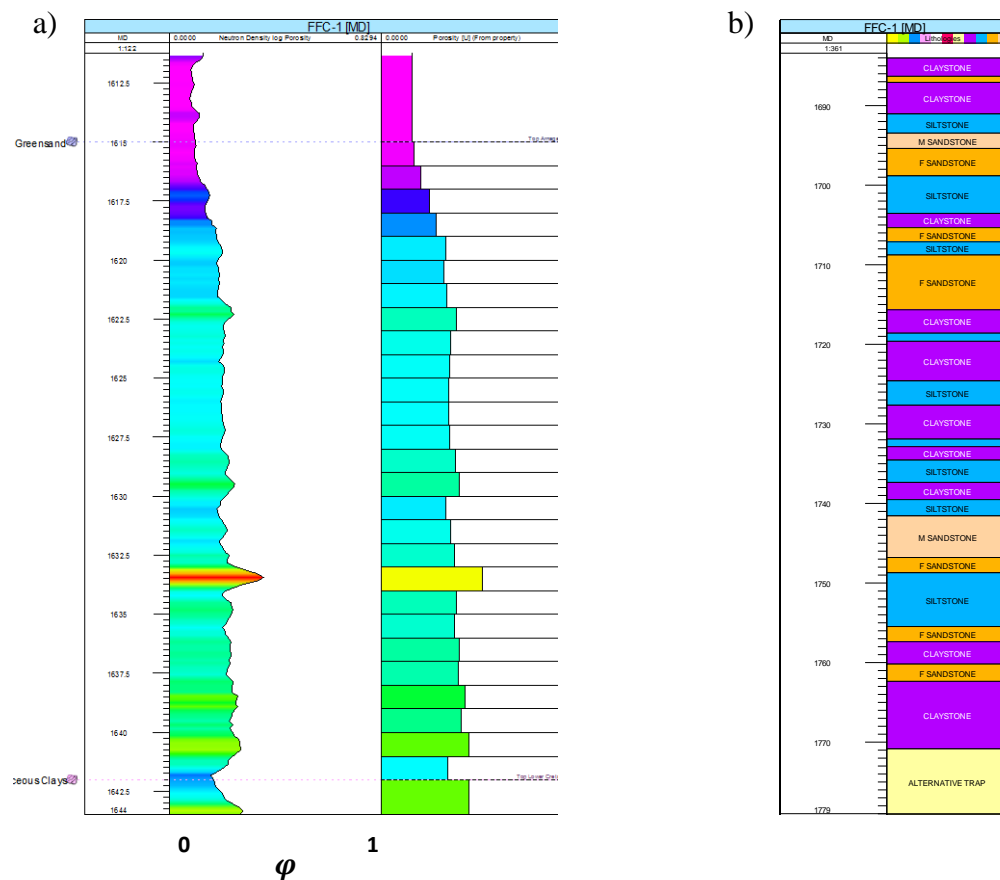


Figure 19. Well logs generated in Petrel using data provided by SGU. a) FFC-1 well section, secondary trap porosity and upscaled porosity. b) Lithology well section of the alternative multilayered trap in FFC-1.

4.8. POROSITY DATA ANALYSIS

The last step in the "porosity data" process was to upscale the porosity from the well grid cells to the entire model with the aim of distributing the porosity from the well log data to the grid cells in the 3D model as realistically as possible preserving the heterogeneity of the geological subsurface. Before the porosity could be modeled the original porosity distribution (fig. 20 a) was transformed into a stationary and normally distributed data set. The reason for removing trends prior modeling was for the input data to be stationary²⁷. The geostatistical algorithm required the input data to be stationary as well as normally distributed with a mean=0 and standard deviation=1. After the data transformation a variogram analysis was made.

4.8.1. Porosity data transformation

The transformation process consisted of the following steps. The output truncation transformation was applied to ensure that the final model did not contain any data outside the specified data range. The minimum and maximum values were set according to table 2. A vertical trend with a correlation factor of -0.71 was detected and extracted (fig. 20 b).

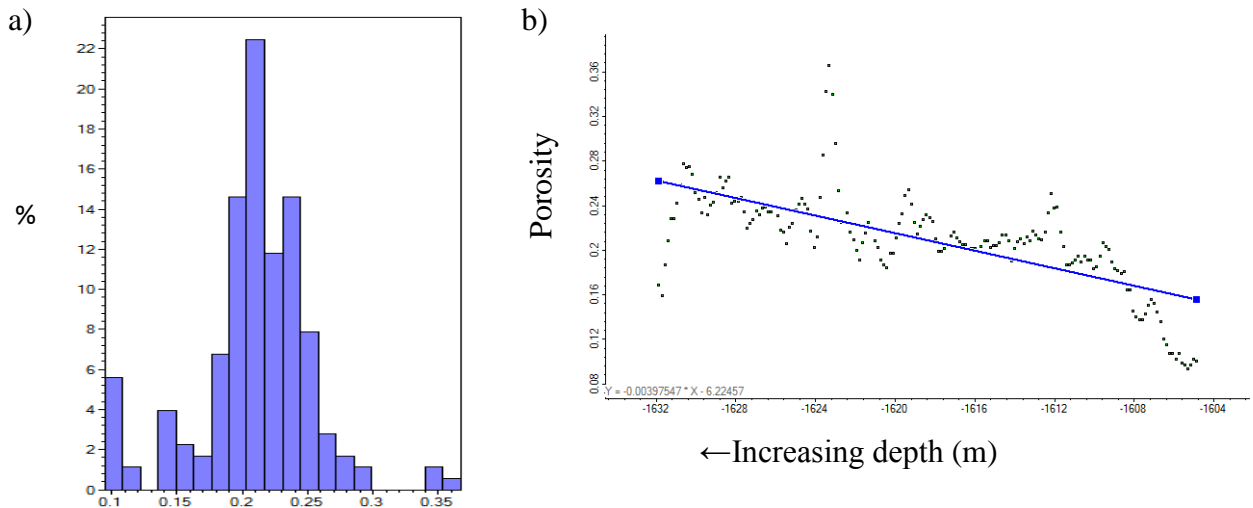


Figure 20. a) Initial porosity distribution. b) Vertical porosity trend.

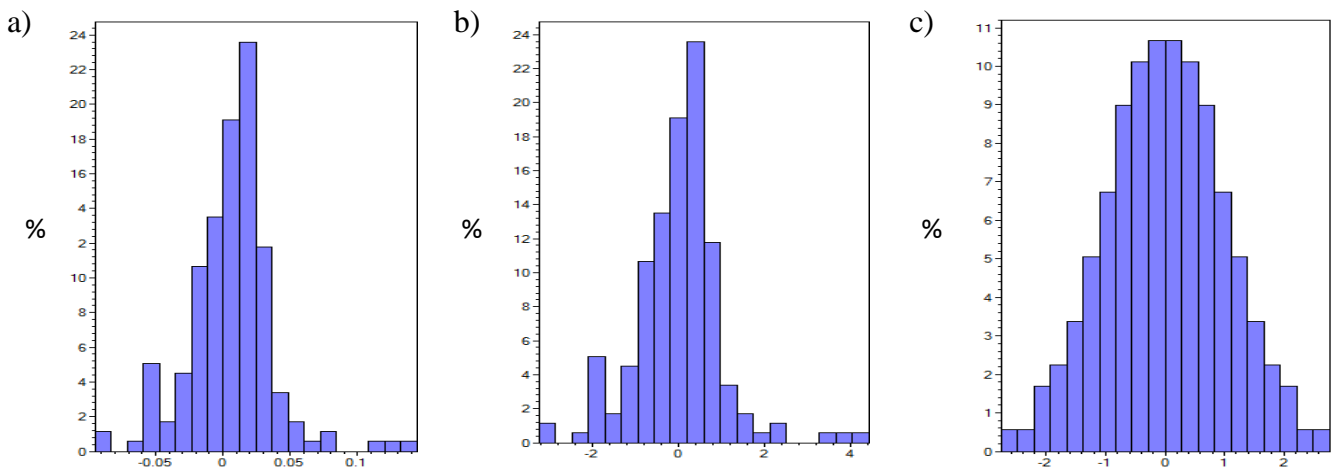


Figure 21. Porosity distribution after : a) 1D trend transformation. b) shift scale transformation. c) normal score transformation.

²⁷ Distribution mean and variance being independent of time and place

After the 1D trend transformation (fig. 21 a) the shift scale transformation was applied to generate a distribution with a mean=0 and standard deviation=1 (fig. 21 b). The normal score transformation was applied to force the distribution into a standard normal distribution (fig. 21 c). After modeling the data was back transformed to its original distribution and the extracted trend was added back on, a procedure performed automatically in Petrel.

4.8.2. Porosity data variogram analysis

A horizontal range could not be computed by variogram analysis but was estimated to 15 000 m based on discussions with Erlström (personal communication). The vertical range was computed to 5.8 m with a nugget of 0.483. The best model fitting was given by the exponential variogram and was therefore selected as model type (fig. 22). A more detailed variogram can be seen in appendix E (fig. E1)

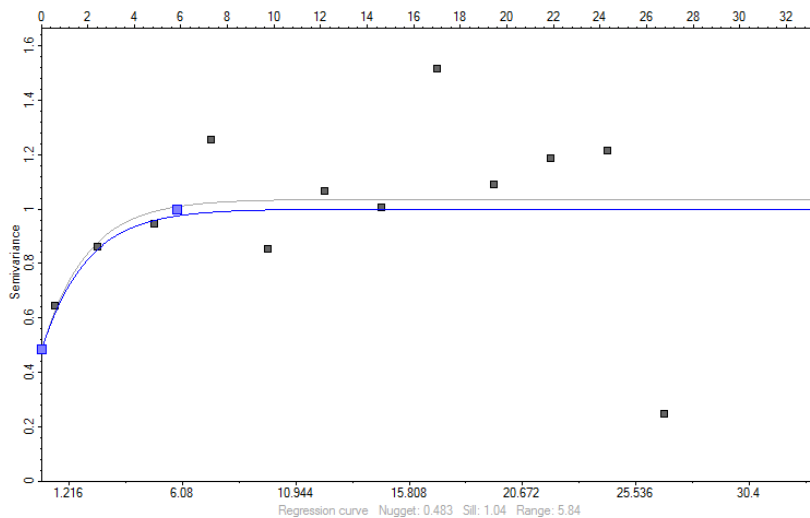


Figure 22. Vertical variogram of porosity with normalized sill for secondary trap.

As can be seen in figure 22 the variogram model line being used in the porosity modeling (blue) does not follow the actual variogram model (grey) but is forced to a sill of 1. Transformed data should have a sill of 1 and if it differs more than +/- 0.3 the data transformation is inaccurate (Schlumberger, 2010).

4.9. FACIES DATA ANALYSIS

Four facies existed in the alternative multilayered trap: Claystone (F_1), siltstone (F_2), fine-grained sandstone (F_3), and medium grained sandstone (F_4) (fig. 23). According to Erlström (personal communication) a natural transition through the sequence of the four facies existed in the alternative multilayered trap: $F_1 \leftrightarrow F_2 \leftrightarrow F_3 \leftrightarrow F_4$. As such the most suitable simulation algorithm to be used was the truncated Gaussian simulation algorithm (*gtsim*) handling such sequence restrictions in the simulation process. The *gtsim* algorithm depended on the *vertical proportion curve*, the *global fraction of each facies* and one *variogram* for all facies.

Like the *gtsim* algorithm the sequential indicator simulation algorithm (*sisim*) also depended on the *vertical proportion curve* and the *global fraction of each facies* the difference being that one specific variogram could be used for each facies. The *sisim* algorithm did not

however handle the sequence restrictions: $F_1 \leftrightarrow F_2 \leftrightarrow F_3 \leftrightarrow F_4$ but was used to increase knowledge of the behavior of facies modeling algorithms.

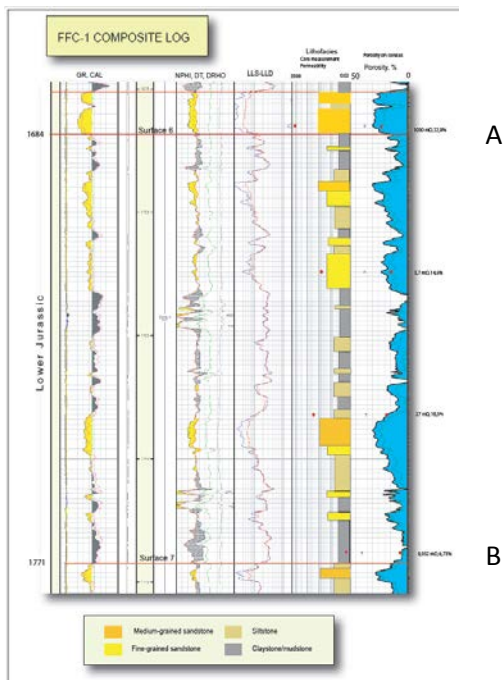


Figure 23. Composite log showing the alternative multilayered trap (between A and B) (Erlström, personal communication).

The probability curve expressed the probability that a certain facies existed in a certain layer. The vertical probability curve (fig. 24 b) was created by the "Fit to linear regression" tool in the facies data analysis process where a straight line trend approximation of the actual facies distribution was created from the upscaled well log (fig. 24 a) which was created on the basis of the FFC-1 composite log (fig. 23).

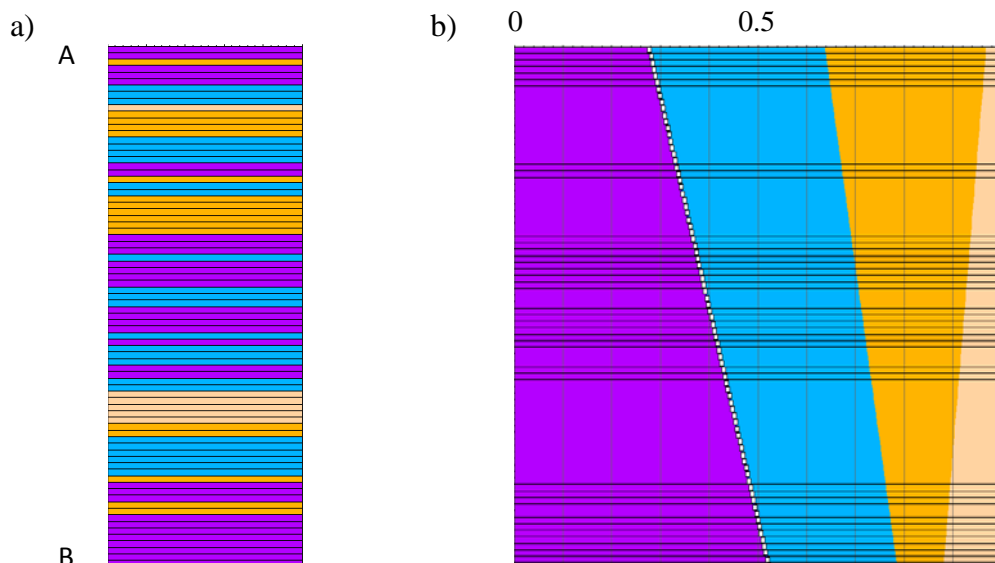


Figure 24. a) Upscaled well log. b) Vertical probability curve.

From the upscaled FFC-1 well log the proportion of claystone was computed to 40%, siltstone 31.25 % fine-grained sandstone 21.25 % and medium-grained sandstone 7.5 %. The facies were ordered in the sequence of $F_1 \leftrightarrow F_2 \leftrightarrow F_3 \leftrightarrow F_4$ (fig. 25). This order determining their location in relation to each other in the final model for *gtsim* but being insignificant for *sisim*.

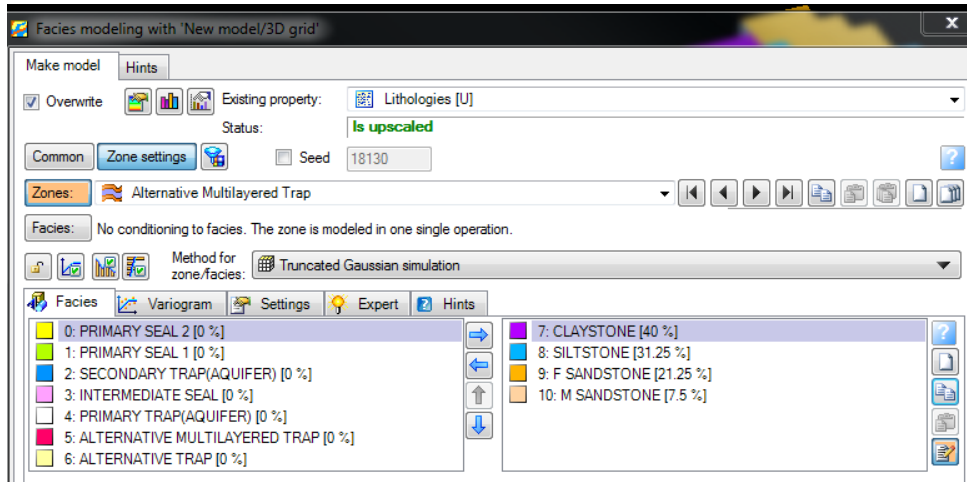


Figure 25. Facies modeling window with the global fractions of each facies.

4.9.1. Gtsim variogram analysis

For the variogram analysis the variogram model chosen was the *Gaussian* model type, the *gtsim* algorithm requiring a *Gaussian* model type. One variogram was set for all facies, Petrel not enabling use of different variograms for different facies when running the *gtsim*.

Horizontal ranges could not be computed but were based on estimations by Erlström (2011) (tab.1). The horizontal ranges were varied in the interval 0.5-30 km in the modeling process.

Table 1. Horizontal range estimations.

Facies	Range (km)
Claystone	>10
Siltstone	2-5
F-gr. Sandstone	2-5
M-gr. Sandstone	5-10

A variogram in the vertical direction (fig. 26) was computed for all facies generating a range of 7.91 m and nugget of 0.486. A more detailed variogram can be seen in appendix E (fig. E2). The default value of range 1 m and nugget of 0 were also used.

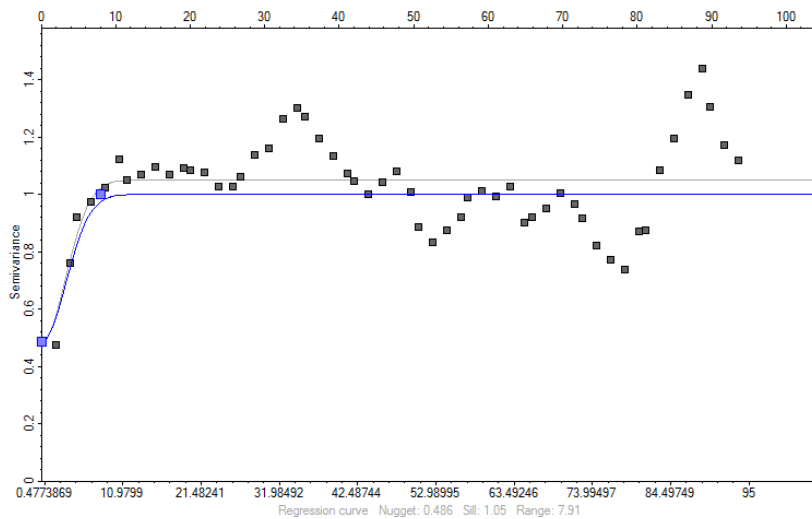


Figure 26. Vertical indicator variogram with normalized sill computed for all facies used.

4.9.2. Sisim variogram analysis

The horizontal ranges were set according to table 1 and the vertical ranges as computed by the vertical variograms (fig. 27 a-d) The spherical variogram model type gave the best fit and was therefore used. More detailed variograms can be seen in appendix E (fig. E3-E6).

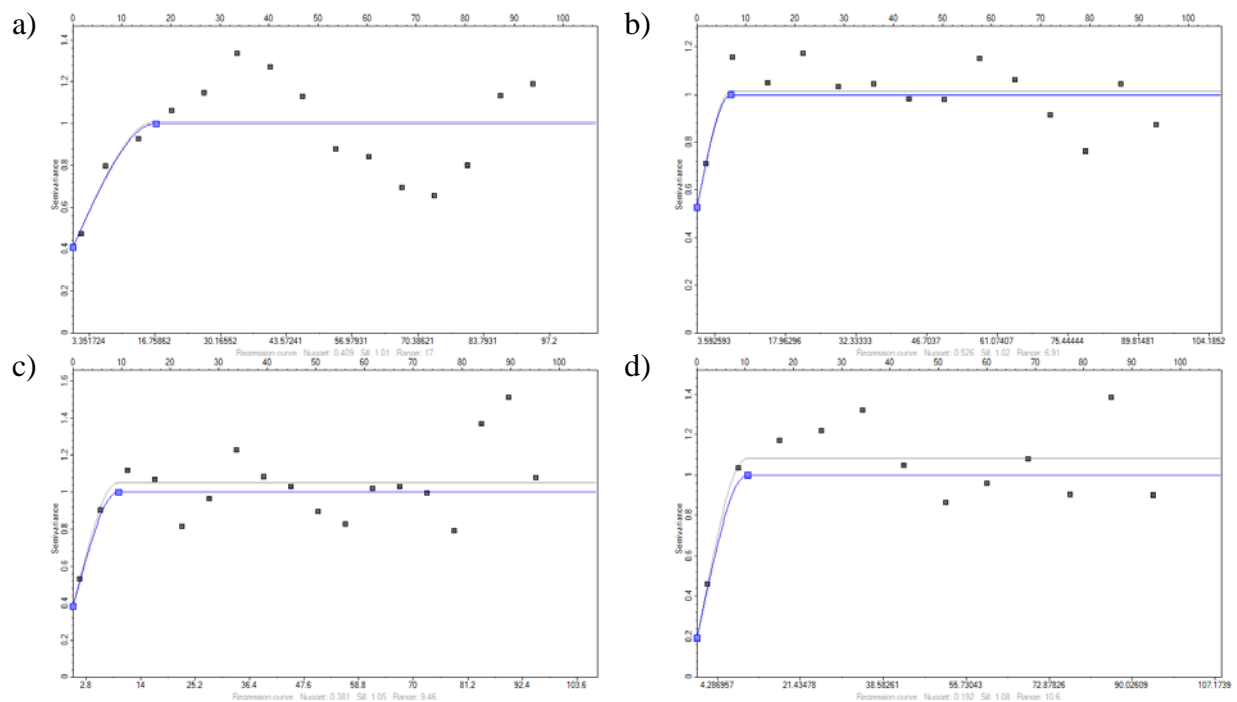


Figure 27. Vertical indicator variogram with normalized sill for: a) claystone. b) siltstone. c) fine grained sandstone. d) medium grained sandstone.

5. RESULTS

5.1. POROSITY STATISTICS

A summary of the FFC-1 porosity statistics can be seen in table 2.

Table 2. Porosity statistics of the FFC-1 well log for the seven zones.

	Min	Max	Delta	N	Mean(μ)	Std (σ)	Var(σ^2)
Primary seal 2	0.0875	0.1298	0.0423	131	0.1053	0.0095	0.0001
Primary seal 1	0.0528	0.131	0.0782	295	0.0922	0.0111	0.0001
Secondary trap	0.0944	0.3667	0.2723	178	0.2093	0.0442	0.002
Intermediate seal	0.1329	0.754	0.6211	210	0.3957	0.2071	0.0429
Primary trap	0.1992	0.2699	0.0707	65	0.2307	0.0159	0.0003
Alternative m.trap	0.1078	0.4677	0.3599	571	0.2079	0.0542	0.0029
Alternative trap	0.1066	0.6152	0.5086	355	0.2432	0.1097	0.012

The figures 28-33 show the histograms, the cumulative density functions (*cdf*) and the normal distributed probability density functions (*pdf*) of the porosity from the FFC-1 well log for the different zones.

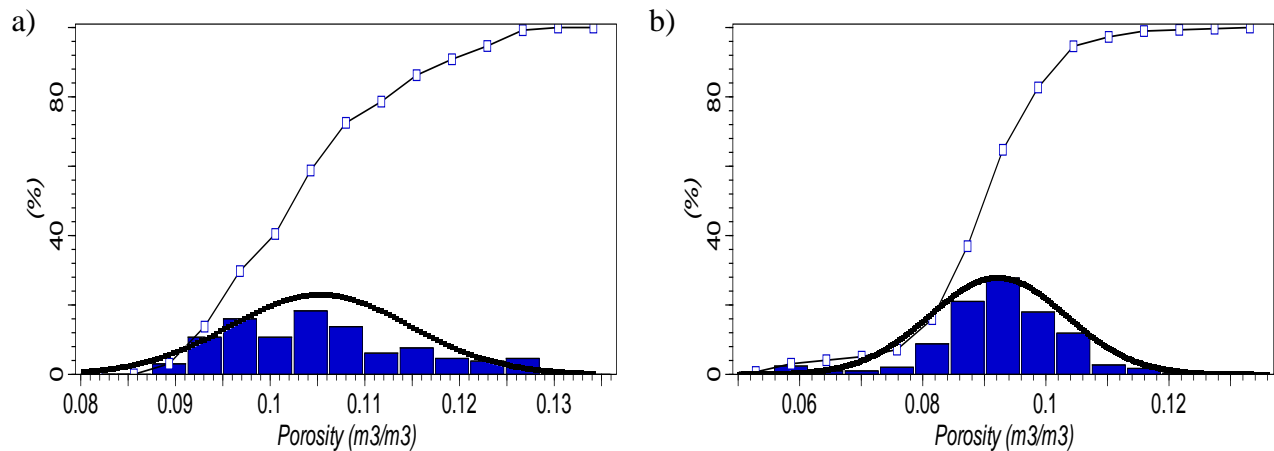


Figure 28. Histogram, *cdf* and *pdf* for: a) Primary seal 2. b) Primary seal 1.

Primary seal 2 (fig. 28 a) is the zone with the second lowest porosity mean ($\mu = 0.1053$) roughly following a normal distribution. Primary seal 1 (fig. 28 b) is the zone with lowest mean ($\mu = 0.0922$) following a normal distribution.

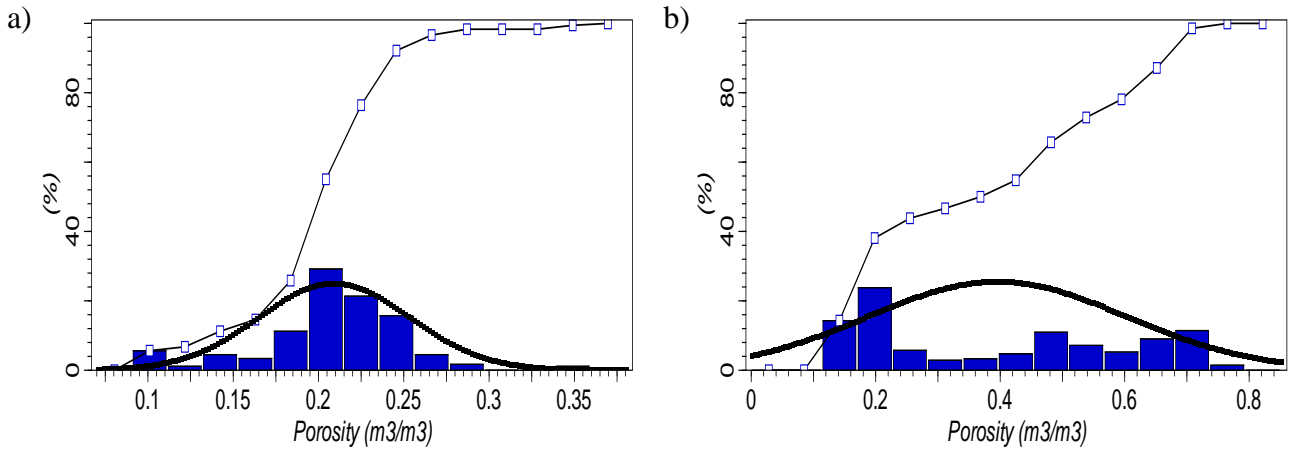


Figure 29. Histogram, *cdf* and *pdf* for: a) Secondary trap. b) Intermediate seal (not trustworthy).

The secondary trap (fig. 29 a) also referred to as the Arnager greensand aquifer and the zone where porosity modeling was performed has a mean porosity of about 20% ($\mu = 0.2093$) roughly following a normal distribution but with some very low porosity values indicating outliers or existence of different facies. The intermediate seal (fig. 29 b) is the zone with the largest variance ($\sigma^2 = 0.0429$) but also the highest mean porosity ($\mu = 0.3957$), the porosity statistics should however not be trusted. According to Erlström a severe washout took place during the intermediate seal measurements explaining the non-normal distribution as well as high porosity and variance.

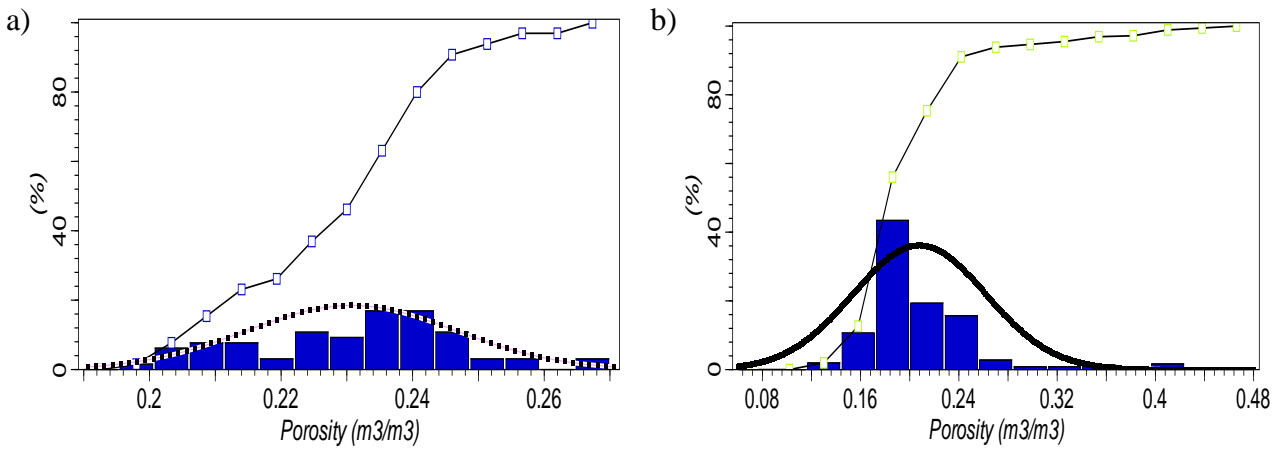


Figure 30. Histogram, *cdf* and *pdf* for: a) Primary trap. b) Alternative multilayered trap.

The primary trap (fig. 30 a) has a mean porosity slightly higher than that of the secondary trap ($\mu = 0.2307$) roughly following a normal distribution. The alternative multilayered trap (fig. 30 b) does not follow the normal distribution which is to be expected knowing the alternative multilayered consists of four different facies each with a significant porosity characteristic.

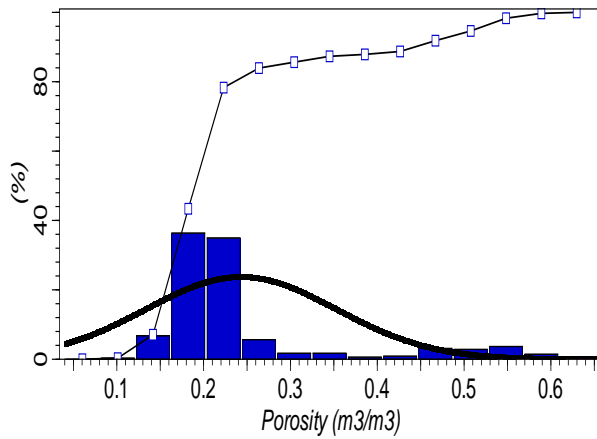


Figure 31. Histogram, *cdf* and *pdf* for the Alternative trap.

The alternative trap (fig. 31) has a similar histogram shape as the alternative multilayered trap indicating the existence of several facies.

5.1.1. Porosity statistics alternative multilayered trap

From figure 30 (b) it could be seen that the alternative multilayered trap porosity distribution did not follow a normal distribution, however this was expected knowing four facies existed in the zone with each facies having a significant porosity characteristic. The FFC-1 composite log (fig. 23) was studied in order to distribute the porosity measurements (fig. 17 c) from the alternative multilayered trap into their respective facies. Summary statistics were computed for each facies separately (tab. 3)

Table 3. Porosity statistics of the alternative multilayered trap.

	Min	Max	Delta	N	Mean(μ)	Std (σ)	Var(σ^2)
Claystone	0.1334	0.4810	0.3475	252	0.2194	0.0708	0.0050
Siltstone	0.1093	0.3621	0.2528	155	0.1960	0.0322	0.0010
F-sandstone	0.1417	0.4738	0.3321	116	0.2124	0.0449	0.0020
M-sandstone	0.1989	0.2665	0.0676	48	0.2482	0.0144	0.0002

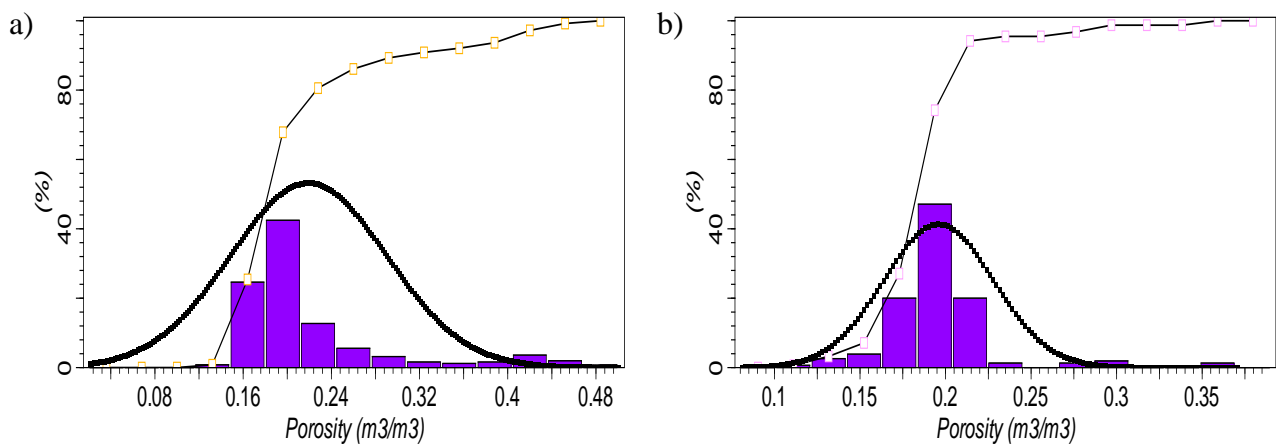


Figure 32. Histogram, *cdf* and *pdf* for: a) claystone. b) siltstone.

The claystone (fig. 32 a) porosity range is very large ($\mu = 0.1334 - 0.4810$)(tab. 3) perhaps indicating the existence of other facies amongst the claystone facies. It has a similar appearance as the alternative multilayered trap with similar statistical values. The siltstone (fig. 32 b) has a mean porosity around 20% ($\mu = 0.1960$) roughly following the normal distribution with some very high porosities $>35\%$

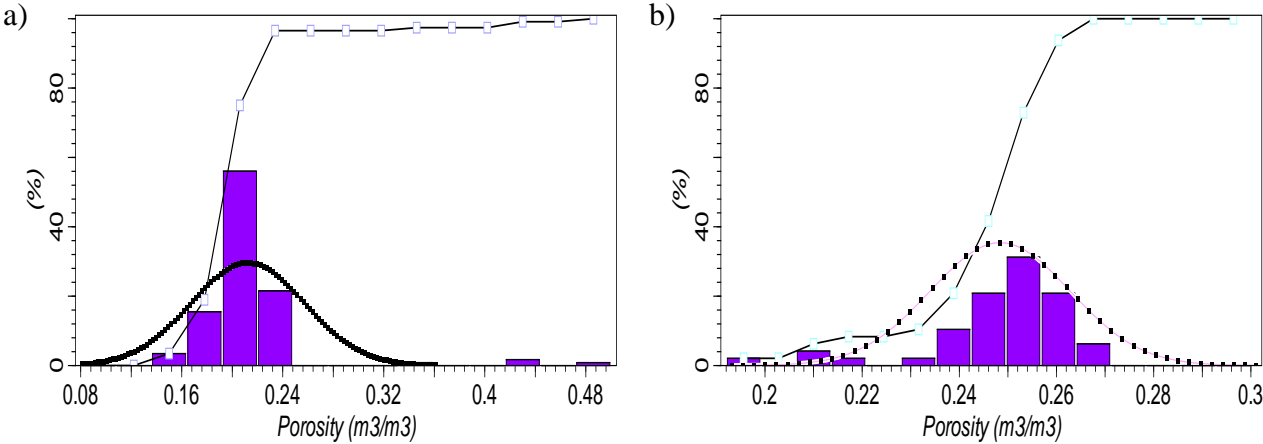


Figure 33. Histogram, *cdf* and *pdf* for: a) Fine-grained sandstone. b) Medium-grained sandstone.

The fine grained sandstone (fig. 33 a) has the second largest porosity range ($\mu = 0.1417 - 0.4738$) however in the porosity interval 25 to 42% no porosity measurements existed indicating outliers. The medium-grained sandstone (fig. 33 a) has the smallest standard deviation ($\sigma = 0.0144$) and largest mean ($\mu = 0.2482$) roughly following the normal distribution.

5.2. STOCHASTIC POROSITY SIMULATION FOR SECONDARY TRAP

The *sgsim* algorithm was used in the porosity modeling process with the transformed data and information from the variogram analysis. 500 realizations ("generally believed to be sufficient" (Van Meirvenne, 2009)) were averaged. Figure 34 (b) shows a single realization of the porosity modeling of the secondary trap and what can be noted are the very sharp transitions between different porosity areas.

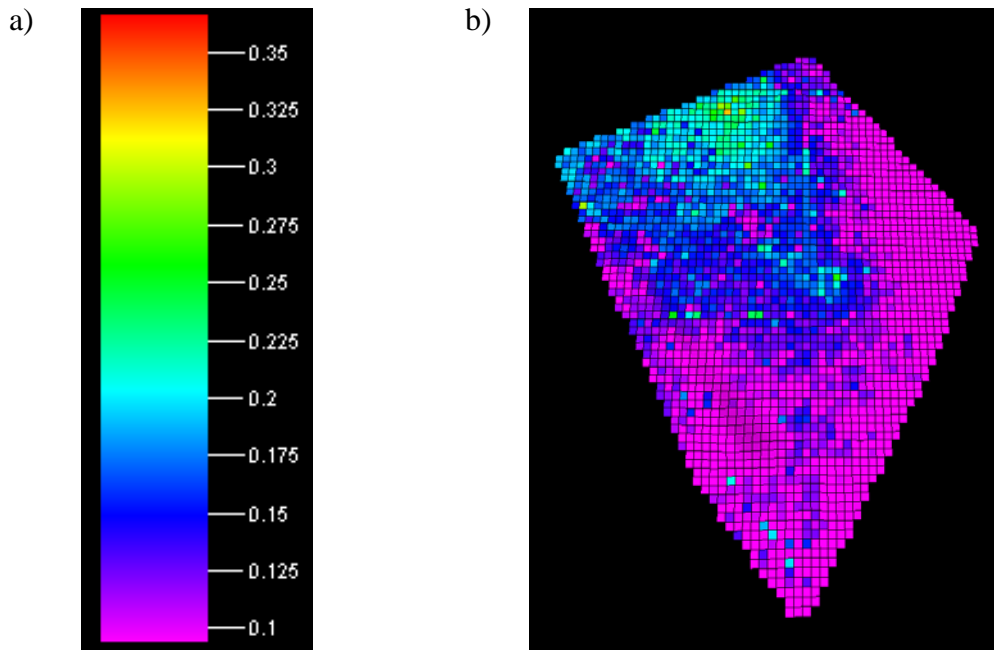


Figure 34. a) Porosity modeling color scale. b) A single realization of the porosity modeling of the secondary trap generated in Petrel using data provided by SGU.

With an average of 500 realizations a much smoother porosity distribution was given. The average distribution however followed that of the single realization to a great extent. Figure 36 shows the realizations of the top layer of the secondary trap (fig. 35) and figure 37 gives a sideways view of the stochastic simulation model, showing the porosity increase with depth.

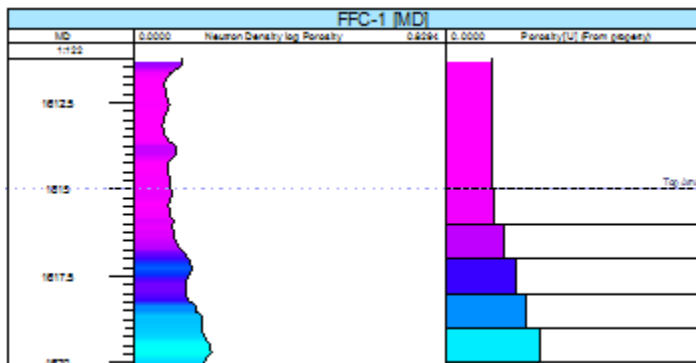


Figure 35. FFC-1 well section showing top layers of secondary trap generated in Petrel using data provided by SGU.

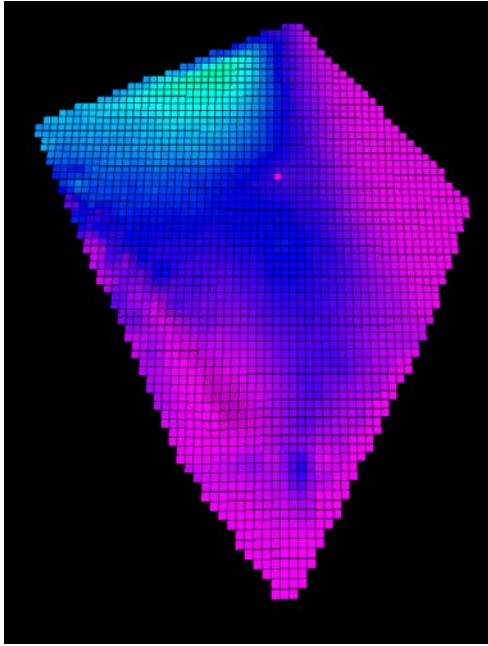


Figure 36. An average of 500 realizations of the porosity modeling of the secondary trap (color scale fig. 34 a) generated in Petrel using data provided by SGU.

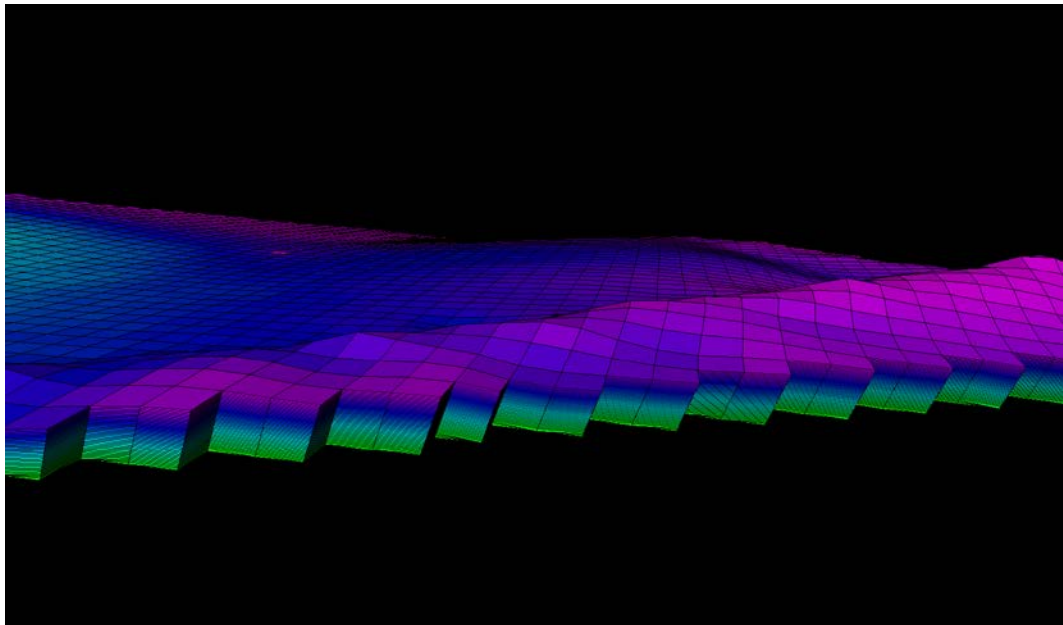


Figure 37. Sideways view in 3D of the averaged secondary trap (color scale fig. 34 a) generated in Petrel using data provided by SGU.

5.3. STOCHASTIC FACIES SIMULATION-GTSIM

Two types of truncated Gaussian simulations were carried out, one with the computed vertical variogram (fig. 26) and one with the default vertical variogram (vertical range=1 m, nugget=0). The horizontal range was varied between 500 and 30000 m.

5.3.1. Gtsim with computed vertical variogram

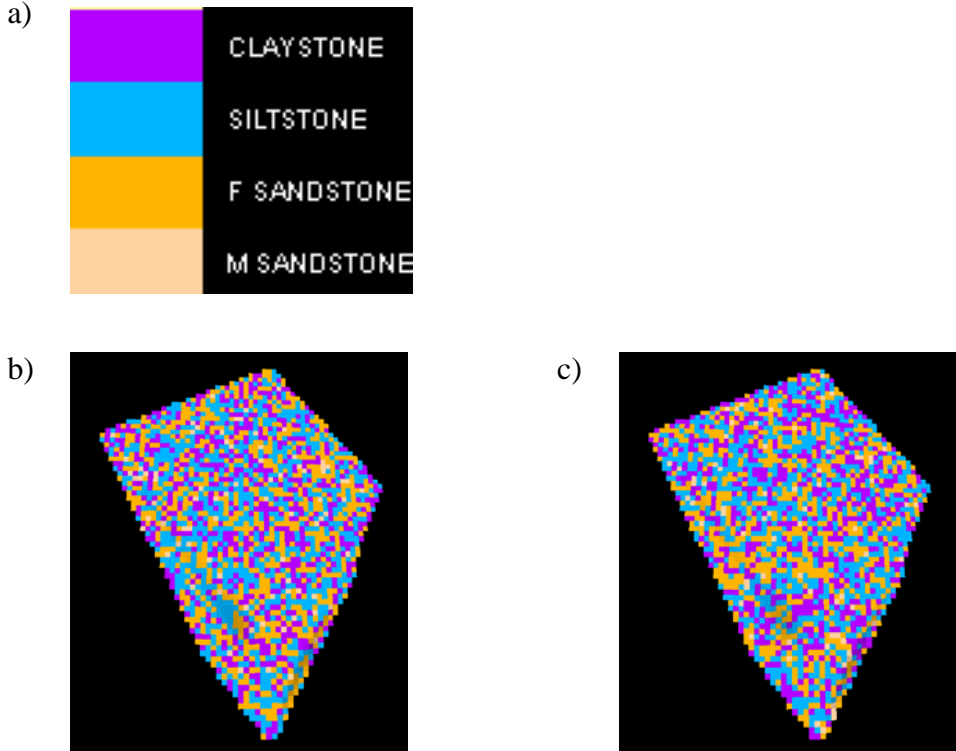
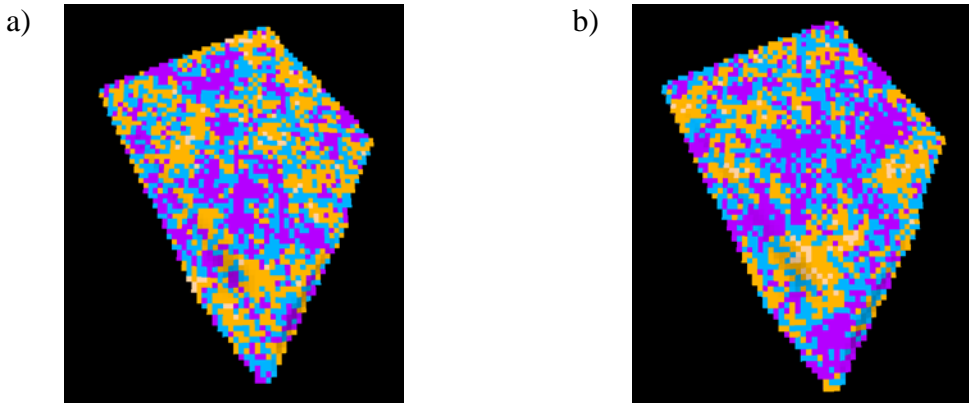


Figure 38. Facies models generated in Petrel using data provided by SGU. a) Facies color scale. b) Facies model generated by using a horizontal range of 500 m. c) Facies model generated by using a horizontal range of 1000 m.

Horizontal ranges of 500 (fig. 38 b) and 1000 m (fig. 38 c) together with the quite large nugget of 0.486 results in a very heterogenic facies distribution not following the natural sequence of : $F_1 \leftrightarrow F_2 \leftrightarrow F_3 \leftrightarrow F_4$ mentioned earlier.



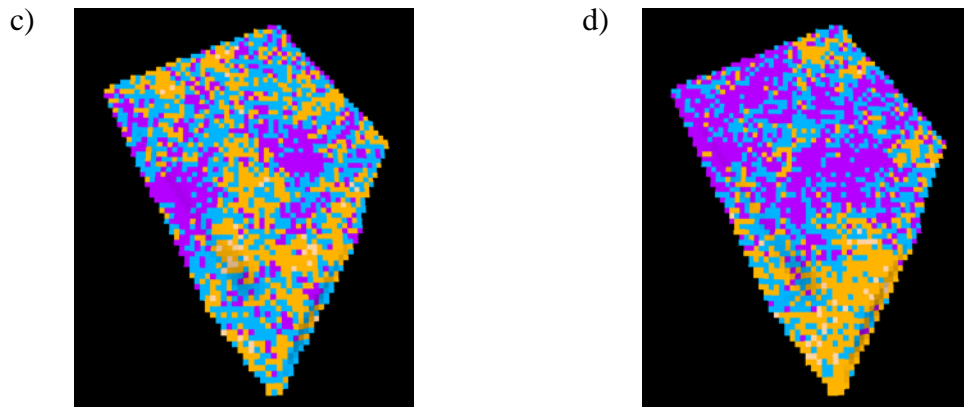


Figure 39. Facies models generated in Petrel using data provided by SGU and a horizontal range of: a) 3500 m. b) 5000 m. c) 10000 m. d) 30000 m.

With a larger horizontal range (fig. 39 a-d) the heterogeneity decreases and the natural sequence of: $F_1 \leftrightarrow F_2 \leftrightarrow F_3 \leftrightarrow F_4$ is followed to a greater extent than previous realizations, however at many locations the natural sequence is not followed.

The heterogeneity does not decrease substantially with a large increase in horizontal range. This probably has its cause in the large nugget "overriding" the effect of the horizontal range. The natural sequence is not followed to a greater extent with a larger horizontal range.

5.3.2. Gtsim with default vertical variogram

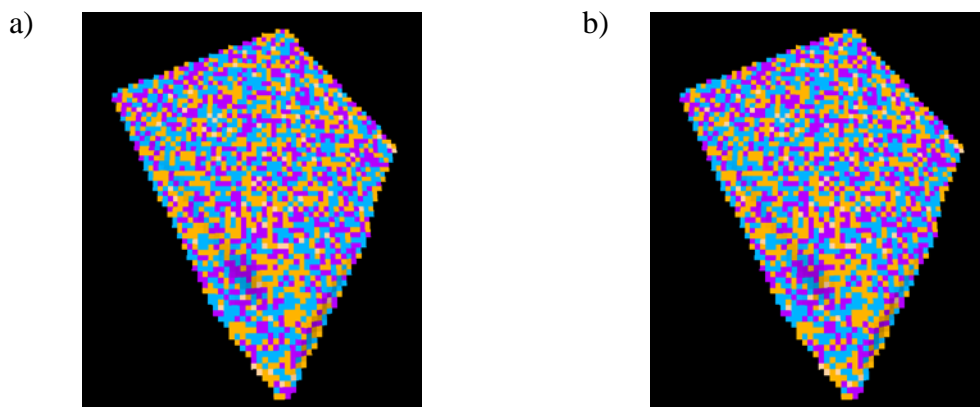


Figure 40. Facies models generated in Petrel using data provided by SGU and a horizontal range of: a) 500 m. b) 1000 m.

The short horizontal ranges (fig. 40 a-b) results in heterogenic realizations with a similar appearance as the corresponding realizations from section 5.3.1.

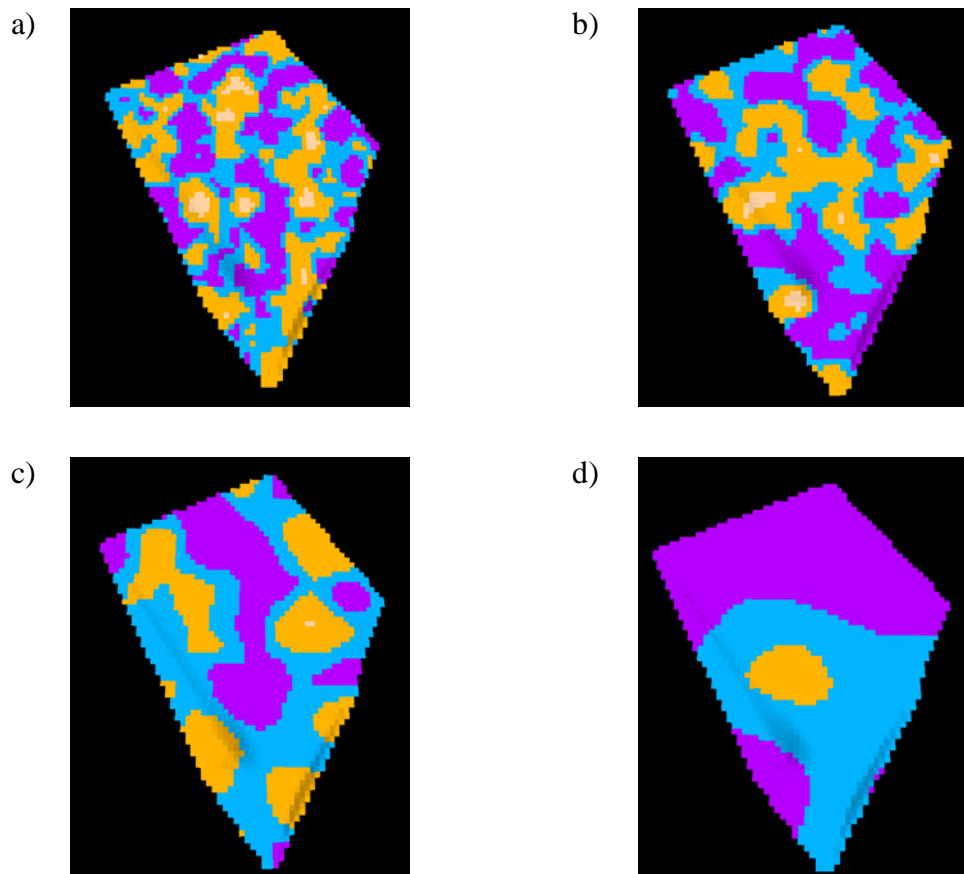


Figure 41. Facies models generated in Petrel using data provided by SGU and a horizontal range of: a) 3500 m. b) 5000 m. c) 10000 m. d) 30000 m.

At a horizontal range of 3500 m (fig. 41 a) a geological reasonable realization (Erlström, personal communication) is given following the natural sequence: $F_1 \leftrightarrow F_2 \leftrightarrow F_3 \leftrightarrow F_4$. With an increase in the horizontal range the heterogeneity decreases and the spatial facies beds grow larger (fig. 41 b-d).

5.4. STOCHASTIC FACIES SIMULATION-SISIM

The *sisim* realizations were carried out with the computed vertical variograms and the horizontal ranges estimated by Erlström (2011) (tab. 1).

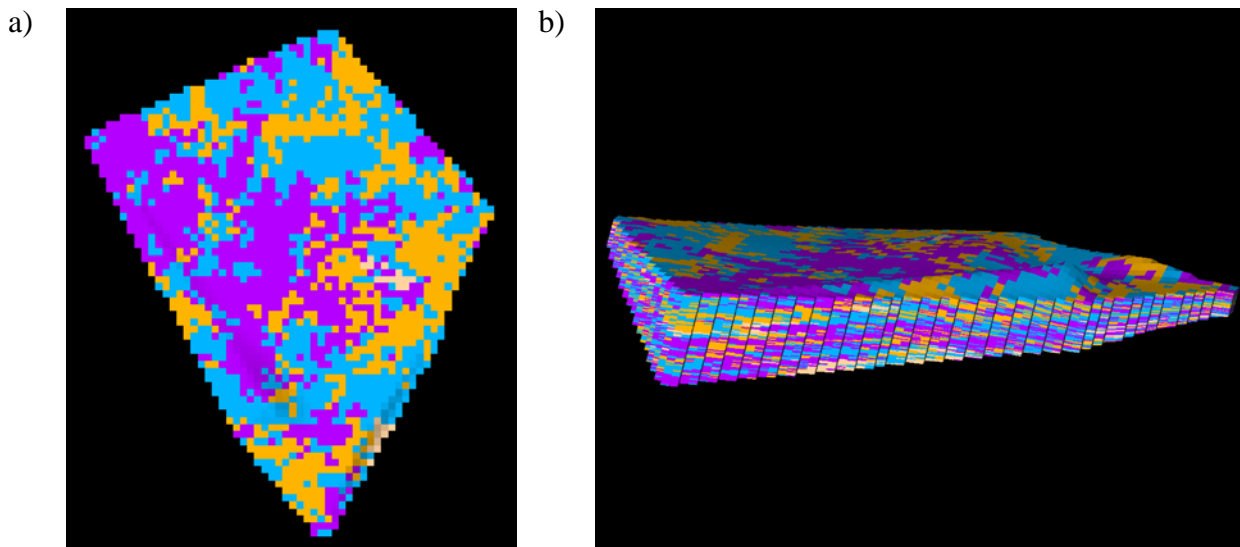


Figure 42. Facies models generated in Petrel using data provided by SGU. a) *Sisim* realization of the top layer. b) Sideways view of the *sisim* realization.

Figure 42 is not geologically reasonable due to the fact that the natural sequence: $F_1 \leftrightarrow F_2 \leftrightarrow F_3 \leftrightarrow F_4$ is not followed at several locations.

5.5. VOLUME CALCULATION

For calculating the bulk and the pore volume (tab. 4) the "Volume calculations" process was used where *bulk volume*=*total rock volume* and *pore volume*=*bulk volume***porosity*.

Table 4. Bulk volume calculations for the south Scania site and the pore volume for the secondary trap.

	Bulk volume($\text{m}^3 \cdot 10^6$)	Pore volume($\text{m}^3 \cdot 10^6$)
Primary Seal 2	413377	-
Primary Seal 1	76118	-
Secondary Trap (Aquifer)	46123	8629
Intermediate seal	39677	-
Primary trap (Aquifer)	15756	-
Alternative Multilayered Trap	152723	-
Alternative Trap	59653	-
Total	803427	-

The pore volume for the remaining traps (tab. 5) was given by: *bulk volume*average porosity* of the corresponding zone.

Table 5. Pore volume for the four traps.

	Pore volume(m³·10⁶)
Secondary trap	8629
Primary trap	3634
Alternative-m trap	31751
Alternative trap	14507
Total	58522

An estimation of the CO₂ storage capacity can be computed by using the model by Szulczewski (2009) or similar.

6. DISCUSSION

It should be pointed out that the major unknown in this study and characteristic for this type of studies in general is that the horizontal correlation structure is essentially unknown and can at best be based on geological estimations. The results should therefore be considered more as a demonstration of the model and of how the horizontal correlation structure of the porosity or of the facies can be, not as exact predictions.

6.1. POROSITY MODELING

The stochastic porosity simulation of the secondary trap reproduced the data with an increase in porosity with depth. The knowledge on the lateral spread of the secondary trap is good. It has been proven in 16 wells by sample analysis. The lateral porosity distribution in the secondary trap is however uncertain. For more precise modeling, porosity-measurements would be needed in several wells to get a better estimation of the lateral porosity distribution and the horizontal range.

The neutron and the density log are measurements of the total porosity. The stochastic porosity simulation of the secondary trap is therefore essentially a total porosity model meaning a model of the sum of the primary porosity and the secondary porosity²⁸. However for CO₂ injection purposes the primary porosity is of main interest. The secondary porosity is less relevant for CO₂ injection purposes since it is not linked with the rest of the porosity matrix and therefore not directly available for storage. Unlike the neutron and the density log the sonic log (appendix C) is a measurement mainly of the primary porosity. Thus an estimation of the secondary porosity can be done by subtracting the neutron-density combination log with the sonic log. However no sonic porosity data was given for the secondary trap. Sonic porosity however is much more unreliable than density and neutron logs and should be calibrated with reference logs such as caliper logs and gamma ray logs (Schlumberger, 2010). Thus for the secondary trap it is not clear how large the secondary porosity is. It could be investigated in possible future work by for example carrying out sonic log measurements where such data do not exist and calibrating existing sonic logs with caliper logs²⁹.

Primary seal 1 and 2 have an average porosity in the FFC-1 well less than half of the average porosity in the subsequent zones. It thus appears that the primary seal 1 and 2 have the impermeable characteristics required for a cap rock. Further porosity measurements in other wells, however, should be carried out as well as permeability measurements for an higher statistical accuracy.

Primary seal 1 and 2, the secondary trap and the primary trap have normal distributed porosities. The intermediate seal, the alternative multilayered trap and the alternative trap do not have normal distributed porosities. A severe wash out³⁰ that took place during logging,

²⁸ Large pore, cavity or void in a rock normally formed by dissolution of minerals (Schlumberger, 2008)

²⁹ The measured diameter of a borehole along its depth (Schlumberger, 2008)

³⁰ An enlarged section of the borehole larger than the drill caused by the collapse rock, mechanical damage of the drill etc (Schlumberger, 2008)

resulting in partly unreliable data is probably the reason for the non normal distribution of the intermediate seal. For the alternative multilayered trap and the alternative trap the existence of different facies, each facies having different porosity characteristics, is the reason for the non normal distribution. Porosity modeling for the alternative multilayered trap and the alternative trap in possible future work should therefore be done by conditioning to facies. Facies modeling must therefore be carried out first.

6.2. TRUNCATED GAUSSIAN SIMULATION

Two types of *gtsim* simulations were carried out, one using a computed vertical variogram and one using a default vertical variogram. The horizontal ranges were equally varied. One of the main drawbacks of *gtsim* was the fact that only one variogram (same for all facies) could be used, leading to all facies having the same range and nugget even though this was not the case. One of the main technical advantages using *gtsim* was that it honored the order between the different facies during certain conditions. A large nugget and small range however overrode the order relation. This was seen when the *gtsim* was used together with the computed variogram where the order sequence of the facies never was honored due to the high computed nugget. When the default vertical variogram was used with a nugget value of 0 and vertical range of 1 m the order was not honored at small horizontal ranges but was honored with larger horizontal ranges. For the alternative multilayered trap to have a facies distribution that is geologically reasonable the nugget needs to be very low. In future work the vertical facies distribution should be investigated in other wells as well, to investigate whether the facies distribution is similar to that in the FFC-1 well, with equally high nuggets.

6.3. SEQUENTIAL INDICATOR SIMULATION

A vertical variogram for each facies was used together with the horizontal range estimations (tab. 1) in the *sisim* process. Thus compared with the *gtsim* process more details of the facies distributions were honored. One major drawback of the use with *sisim* was the fact that the order between the facies was not honored by the algorithm. An algorithm honoring order between facies as well as enabling the use of facies-linked variograms would be ideal for this kind of modeling.

6.4. VOLUME CALCULATION

The computed total pore volumes of the four traps should be viewed as rough estimations. Further porosity sampling and investigations regarding the secondary porosity as well as modeling of the remaining three traps as well as re-modeling of the secondary trap is required to get a better statistical accuracy of the pore volume available for CO₂ storage. To gain knowledge on the storage capacity injection simulations and further studies are required.

7. REFERENCES

- Bachu, S. 2007. CO₂ storage in geological media: Role, means, status and barriers to deployment. *Progress in Energy and Combustion Science*, Volume 34, Issue 2, 254-273. ISSN 0360-1285.
- Bachmaier, M., Backes, M. 2008. Variogram or semivariogram? Understanding the variances in a variogram, *Precision Agric*, Volume 9, Issue 3, 173–175
- CO2CRC. 2011. About CCS. Website (11/5 -11), <http://www.co2crc.com.au/aboutccs/index>
- Deutsch, C.V., Journel, A.G. 1998. *GSLIB. Geostatistical Software Library and User's Guide*, 2nd. Oxford, New York: Oxford University Press. ISBN 0 19 510015 8
- Dewan, J.T. 1983. *Essentials of modern open-hole log interpretation*, PennWell Books, Tulsa, Okla.
- DOE. 2011. Enhanced Oil Recovery/CO₂ Injection. Website (11/5 -11), <http://www.fossil.energy.gov/programs/oilgas/eor/index.html>
- Erlström, M., Fredriksson, F., Juhojuntti, N., Sivhed, U., Wickström, L. 2011. Lagring av koldioxid i berggrunden - krav, förutsättningar och möjligheter. Geological Survey of Sweden. ISSN 1652-8336.
- IEA. 2010. CO₂ Emissions From Fuel Combustion - Highlights. OECD/IEA, Paris.
- IPCC. 2005. Carbon dioxide capture and storage. Cambridge University Press, Cambridge.
- IPCC. 2007. Summary for Policymakers. In: *Climate Change 2007: The Physical Science Basis*. Cambridge University Press, Cambridge, U.K and New York, USA.
- Journel, A.G., Ying, Z. 2001. The theoretical links between sequential Gaussian simulation, Gaussian truncated simulation, and probability field simulation. *Mathematical Geology*, Volume 33, No. 1, 2001.
- Lyons, W.C., Plisga, G.J. 2005. *Standard Handbook of Petroleum and Natural Gas Engineering*, 2nd ed. Elsevier, Oxford
- Michael, K., Golab, A., Shulakova, V., Ennis-King, J., Allinson, G., Sharma, S., Aiken, T. 2010. Geological storage of CO₂ in saline aquifers - A review of the experience from existing storage operations. *International Journal of Greenhouse Gas Control*, Volume 4, Issue 4, 659-667. ISSN 1750-5836.
- Pires, J.C.M., Martins, F.G., Alvim-Ferraz, M.C.M., Simões, M. 2011. Recent developments on carbon capture and storage: An overview. *Chem. Eng. Res. Des.* Volume 89, Issue 9, 1446-1460. ISSN 0263-8762.
- Schlumberger. 1991. *Log Interpretation Principles/ Applications*. Schlumberger Educational Services, Houston

Schlumberger. 2008. Oil Field Glossary. Website (11/5 - 11), <http://www.glossary.oilfield.slb.com/>

Schlumberger. 2010. Petrel technical manual.

Serra, O. 1984. *Fundamentals of Well-Log Interpretation - The Acquisition of Logging Data*. Elsevier, Amsterdam

SGU. 2010. Sveriges berggrund (bedrock of Sweden). Website (11/5 - 11), http://www.sgu.se/sgu/sv/geologi/svberg_s.htm

Szulczewski, M., Juanes, R. 2009. A simple but rigorous model for calculating CO₂ storage capacity in deep saline aquifers at the basin scale, *Energy Procedia*, Volume 1, Issue 1, 3307-3314, ISSN 1876-6102

Vann, J., Bertoli, O. and Jackson, S., 2002. An overview of geostatistical simulation for quantifying risk. Proceedings of the geostatistical association of Australia symposium "Quantifying risk and error"

Van Meirvenne, M., Meklit, T. 2010. Geostatistical Simulation for the Assessment of Regional Soil Pollution. *Geographical Analysis*, Volume 42, Issue 2, 121-135. ISSN 0016-7363

Vattenfall. 2010a. Capture of CO₂-Precombustion Capture. Website (11/5 -11), <http://www.vattenfall.com/en/ccs/precombustion.htm>

Vattenfall. 2010b. Capture of CO₂- Oxyfuel combustion Capture. Website (11/5 -11), <http://www.vattenfall.com/en/ccs/oxyfuel-combustion.htm>

Wurdemann, H., Moller, F., Kuhn M., Heidug W., Christensen, N.P., Borm, G., Schilling, F.R. 2010. From site characterisation and risk assessment to monitoring and verification: One year of operational experience with the field laboratory for CO₂ storage at Ketzin, Germany. *International Journal of Greenhouse Gas Control*, Volume 4, Issue 6, 938-951. ISSN 1750-5836.

Personal communication

Erlström, Mikael, State geologist, SGU (2011)

APPENDIX A

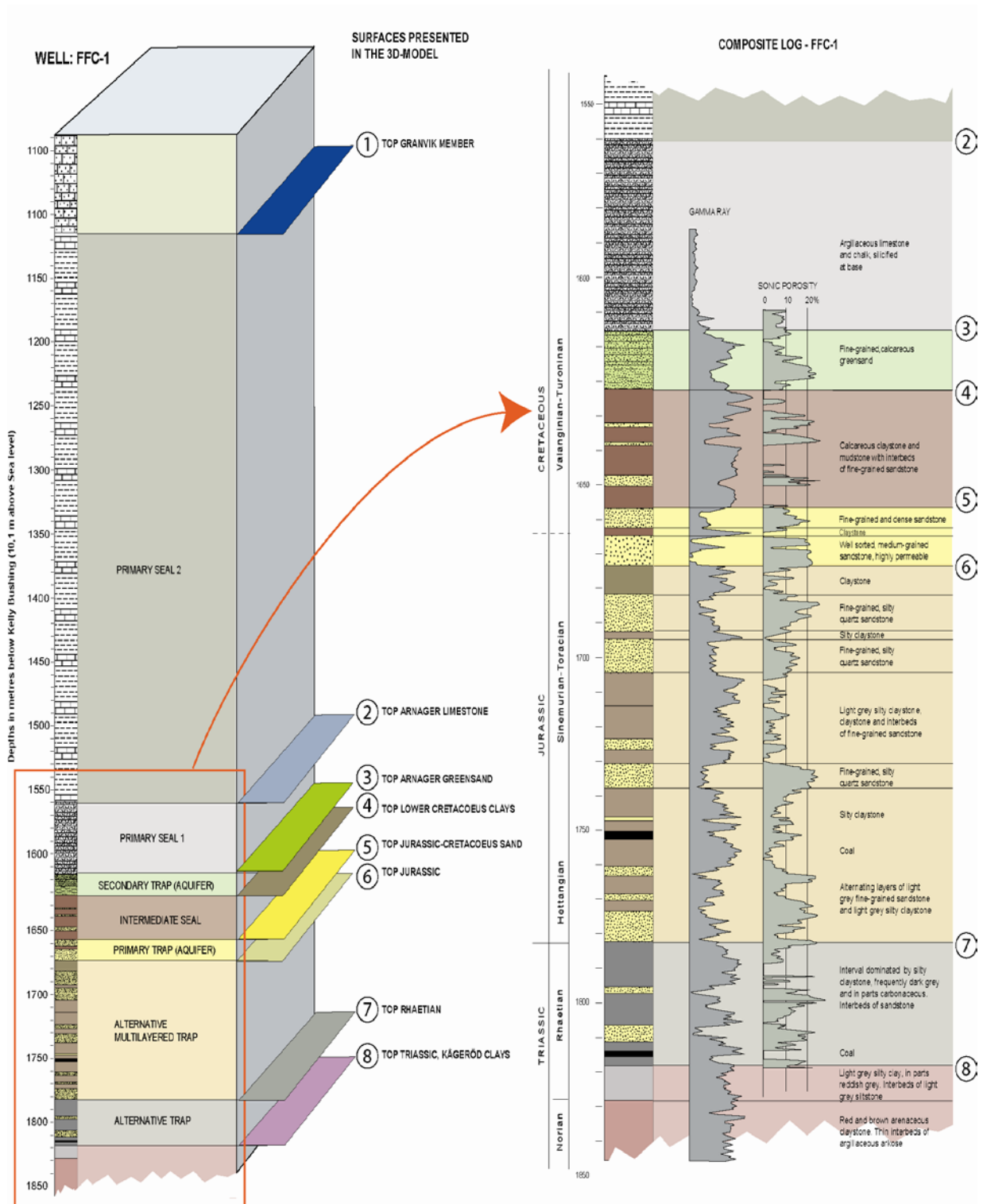


Figure A. A cross section of the formation at FFC-1 (Erlström, personal communication).

APPENDIX B

a) Surface 3 TOP ARANGER SAND - Notepad

File	Edit	Format	View	Help
1324500	6135000	-1107,45		
1323000	6136500	-1117,15		
1324500	6136500	-1130,82		
1326000	6136500	-1133,79		
1323000	6138000	-1140,51		
1324500	6138000	-1153,55		
1326000	6138000	-1156,09		
1321500	6139500	-1150,21		
1323000	6139500	-1163,88		
1324500	6139500	-1177,14		
1326000	6139500	-1183,74		
1327500	6139500	-1183,49		
1320000	6141000	-1159,9		
1321500	6141000	-1173,57		
1323000	6141000	-1187,24		
1324500	6141000	-1200,74		
1326000	6141000	-1209,88		
1327500	6141000	-1194,72		
1318500	6142500	-1169,59		
1320000	6142500	-1183,26		
1321500	6142500	-1196,85		
1323000	6142500	-1210,3		
1324500	6142500	-1221,12		
1326000	6142500	-1235,96		
1327500	6142500	-1220,6		
1329000	6142500	-1233,19		
1317000	6144000	-1179,28		
1318500	6144000	-1192,96		
1320000	6144000	-1205,29		
1321500	6144000	-1217,27		
1323000	6144000	-1225,72		
1324500	6144000	-1240,53		
1326000	6144000	-1257,61		
1327500	6144000	-1242,99		
1329000	6144000	-1245,49		
1330500	6144000	-1271,65		
1317000	6145500	-1186,53		
1318500	6145500	-1198,08		
1320000	6145500	-1206,48		
1321500	6145500	-1222,05		
1323000	6145500	-1241,55		
1324500	6145500	-1260,92		
1326000	6145500	-1271,94		

X Y Z

b) E1793

	A	B	C	D
1	Djup m KB	Neutron Porosit	Sonic porosit	Bulk density log
2	1550.07	0.11	-999.25	2.46
3	1550.23	0.11	-999.25	2.44
4	1550.38	0.12	-999.25	2.44
5	1550.53	0.12	-999.25	2.44
6	1550.68	0.13	-999.25	2.44
7	1550.84	0.12	-999.25	2.44
8	1550.99	0.11	-999.25	2.45
9	1551.14	0.11	-999.25	2.44
10	1551.29	0.11	-999.25	2.43
11	1551.45	0.11	-999.25	2.44
12	1551.60	0.12	-999.25	2.44
13	1551.75	0.11	-999.25	2.43
14	1551.90	0.12	-999.25	2.44
15	1552.06	0.12	-999.25	2.44
16	1552.21	0.11	-999.25	2.44
17	1552.36	0.11	-999.25	2.45

Depth(m) φ_n φ_s ρ_B

Figure B1. a) XYZ format data describing surface 3, top Arnager green sand. b) Well log containing porosity information. -999.25 means missing data.

H	I	J	K	L	M	N
Top Granvik Member			Top Arnager Limestone			Top Arnager g
Surface 1			Surface 2			Surface 3
Top seal 2			Top seal 1			Top secondary
			Base seal 2			Base seal 1
m b. KB	m b sl	Thickness	m b. KB	m b sl	Thickness	m b. I
1258	1250	428	1686	1678	48	1734
1020	990	279	1299	1269	84	1383
1125	1115	445	1570	1560	45	1615
963	955	184	1147	1139	65	1212
900	892	234	1134	1126	64	1198
975	957	283	1258	1240	75	1333
884	880	252	1136	1132	53	1189
975	971	229	1204	1200	74	1278
882	877	241	1123	1118	62	1185
925	907	263	1188	1170	61	1249
1285	1275	262	1547	1537	54	1601
1406	1370	239	1645	1609	65	1710
1330	1313	433	1763	1746	25	1788
810	787	205	1015	992	80	1095
1197	1150	219	1416	1369	66	1482
1240	1230	826	2066	2056	80	2146
		314			63	

Figure B2. Depth information and location of wells.

APPENDIX C

SONIC LOG

A sonic log is made from measurements of the speed of sound (Serra, 1984). A sound wave in the frequency area of 20 to 40 kHz is emitted by a transmitter in very short thrusts, 10 to 60 times per second. The speed in which the sonic wave traverses the formation is dependent on the lithology and porosity of the formation. For consolidated and compacted sandstones which is the case in the South Scania site aquifers the sonic porosity (φ_{so}) can be expressed by the Wyllie Time-Average Equation $\varphi_{so} = \frac{t_{LOG} - t_{ma}}{t_f - t_{ma}}$ where t_{LOG} is the reciprocal of the sonic velocity read from the sonic log, t_{ma} the transit time of the matrix material and t_f the transit time of the saturating fluid (Lyons, 2005).

The sound emission establishes P-waves, S-waves, surface waves and guided waves in the formation. The first wave to be picked up by the receiver is the P-wave also called the compressional wave, it travels from the transmitter to the borehole wall where it is refracted, it then travels within the formation at the compressional wave velocity of the formation and then finally to the receiver as a fluid pressure wave (Lyons, 2005). The second wave to be picked up by the receiver is the S-wave which has the same travel path but instead of traveling with the compressional wave velocity in the formation it travels with the shear wave velocity.

Sonic porosity (φ_{so}) is a measurement mainly of the primary porosity and is quite insensitive to secondary porosity such as fractures and vugs. Neutron and density log porosity however do not distinguish in type of porosity thus the secondary porosity can be calculated by $\varphi_s = \varphi - \varphi_{so}$.

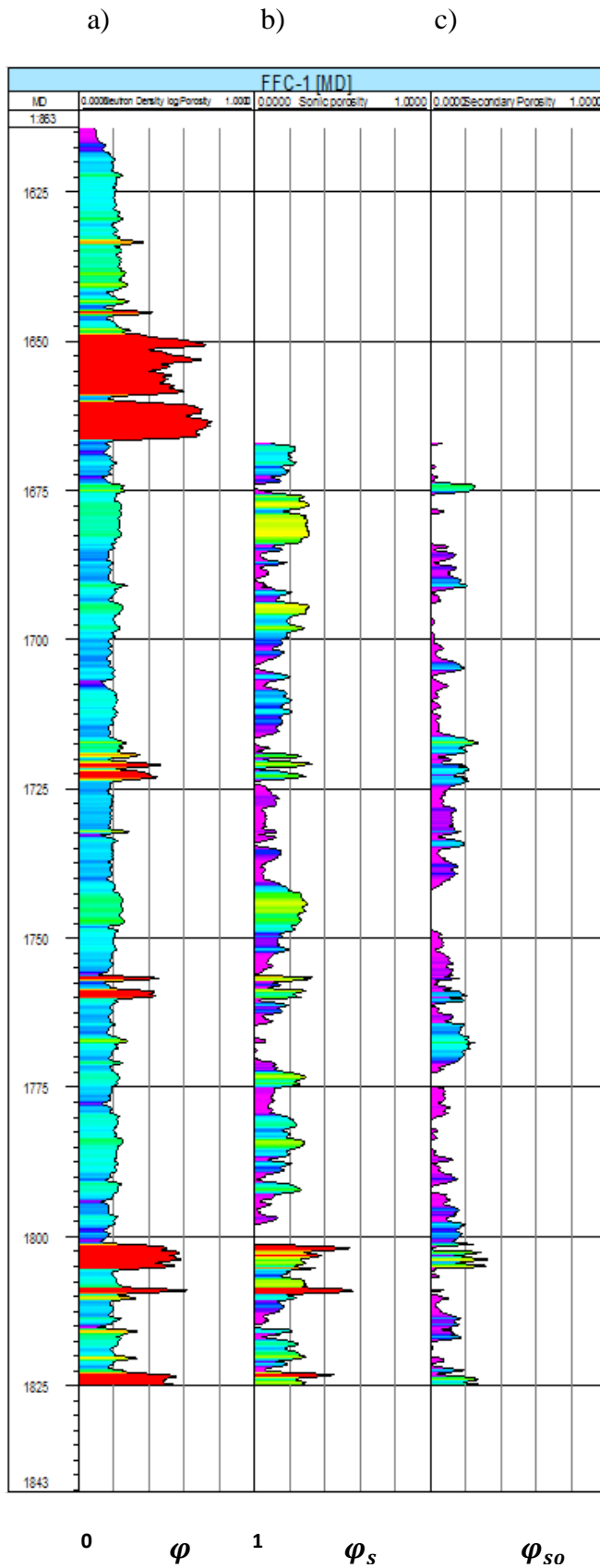


Figure C. Well logs generated in Petrel using data provided by SGU. a) Combined density log/neutron porosity. b) uncalibrated sonic log porosity. c) uncalibrated secondary porosity in FFC-1 well section.

APPENDIX D

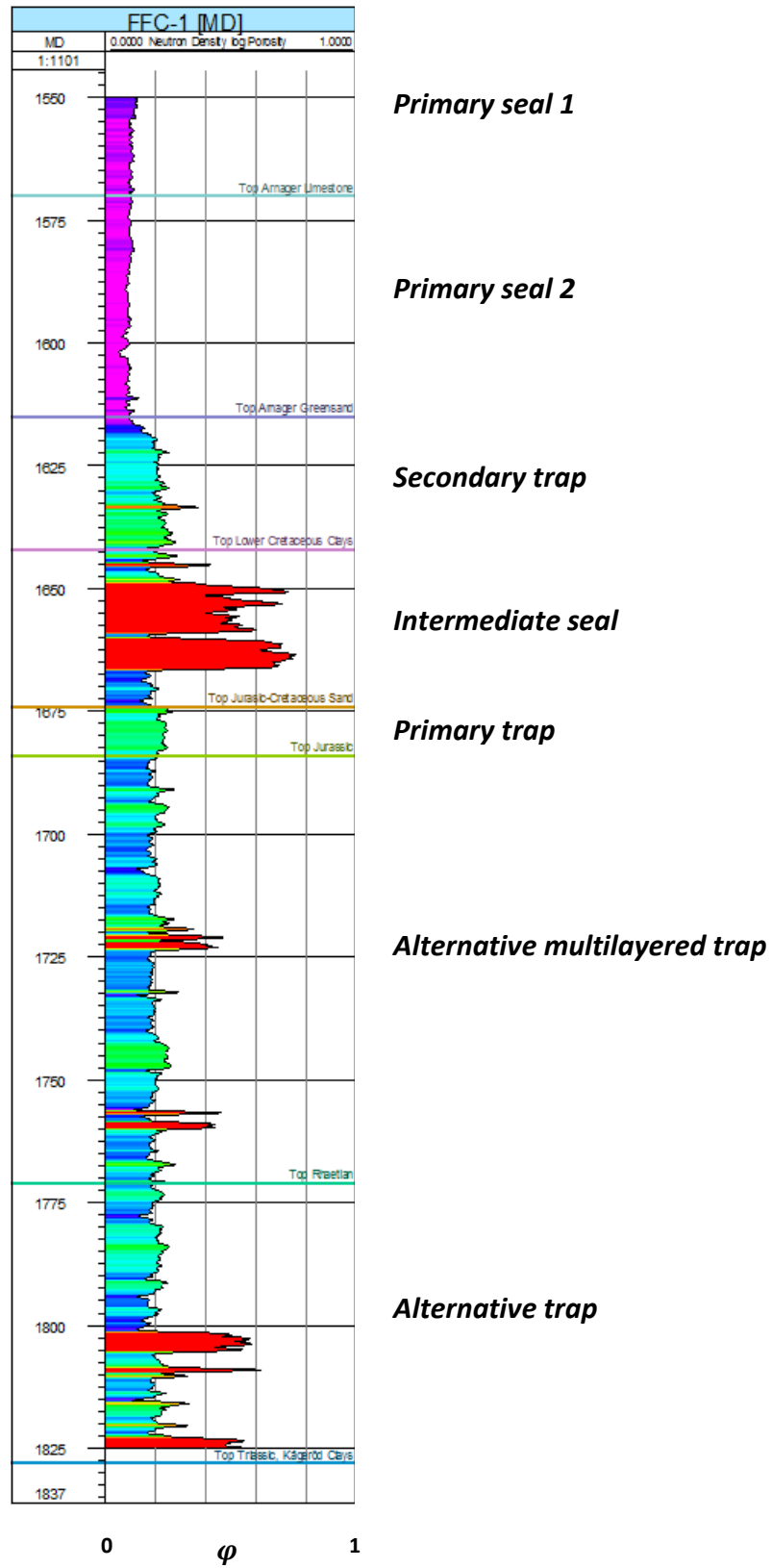


Figure D. Combined density log/neutron porosity from FFC-1 with zones generated in Petrel using data provided by SGU.

APPENDIX E

The histograms in the variograms show the number of sample pairs in each lag.

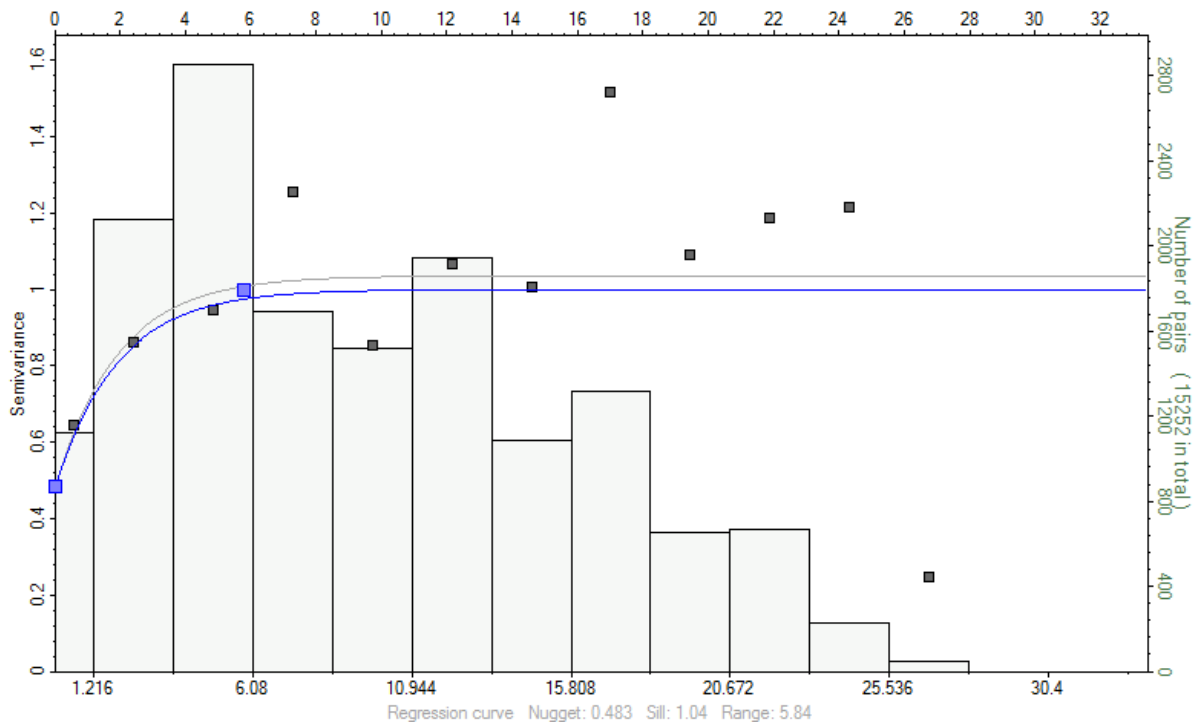


Figure E1. Vertical variogram of porosity with normalized sill for the secondary trap with a lag distance of 2.4 m. Generated in Petrel using data provided by SGU.

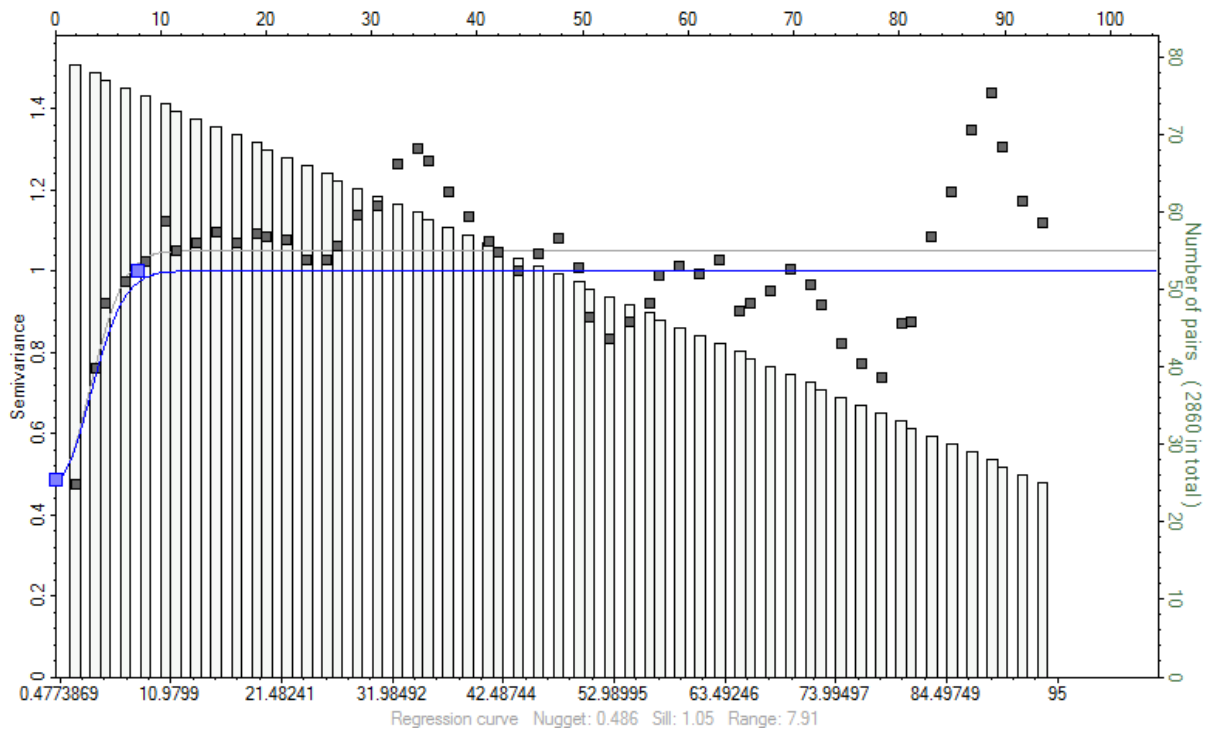


Figure E2. Vertical indicator variogram with normalized sill computed for all facies used for the alternative multilayered trap with a lag distance of 1 m. Generated in Petrel using data provided by SGU.

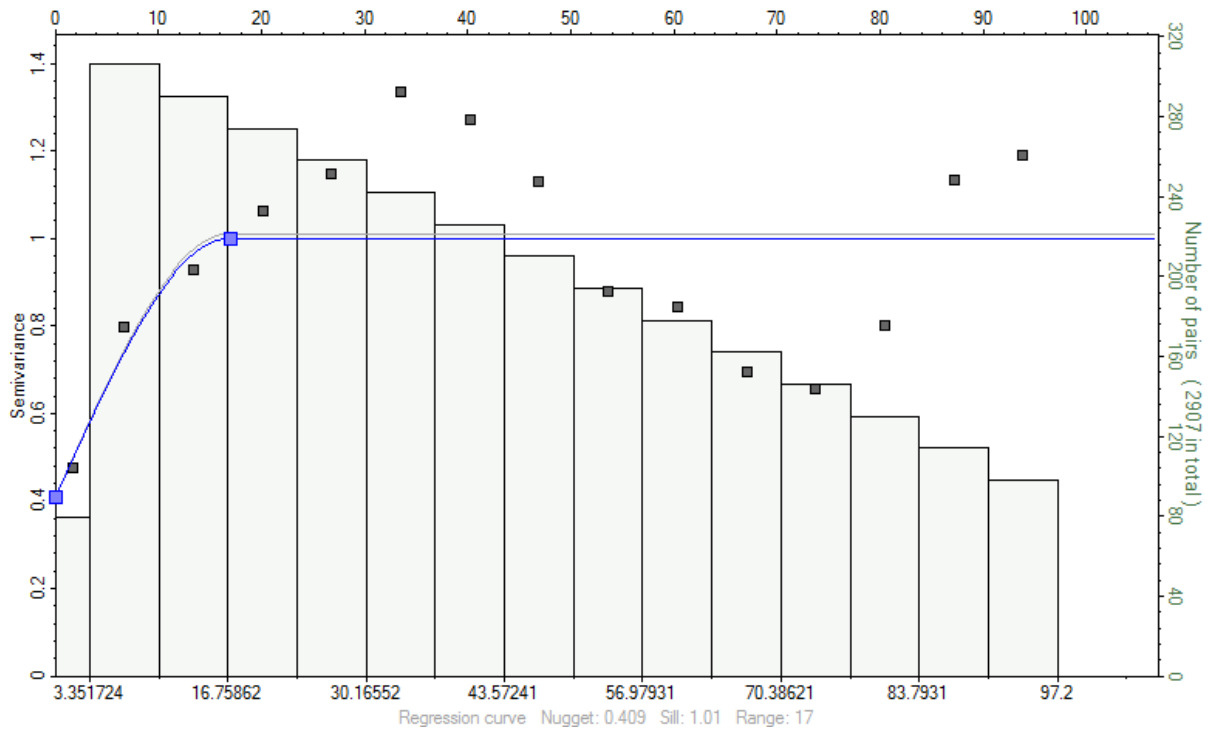


Figure E3. Vertical indicator variogram with normalized sill computed for claystone in the alternative multilayered trap with a lag distance of 6.7 m. Generated in Petrel using data provided by SGU.

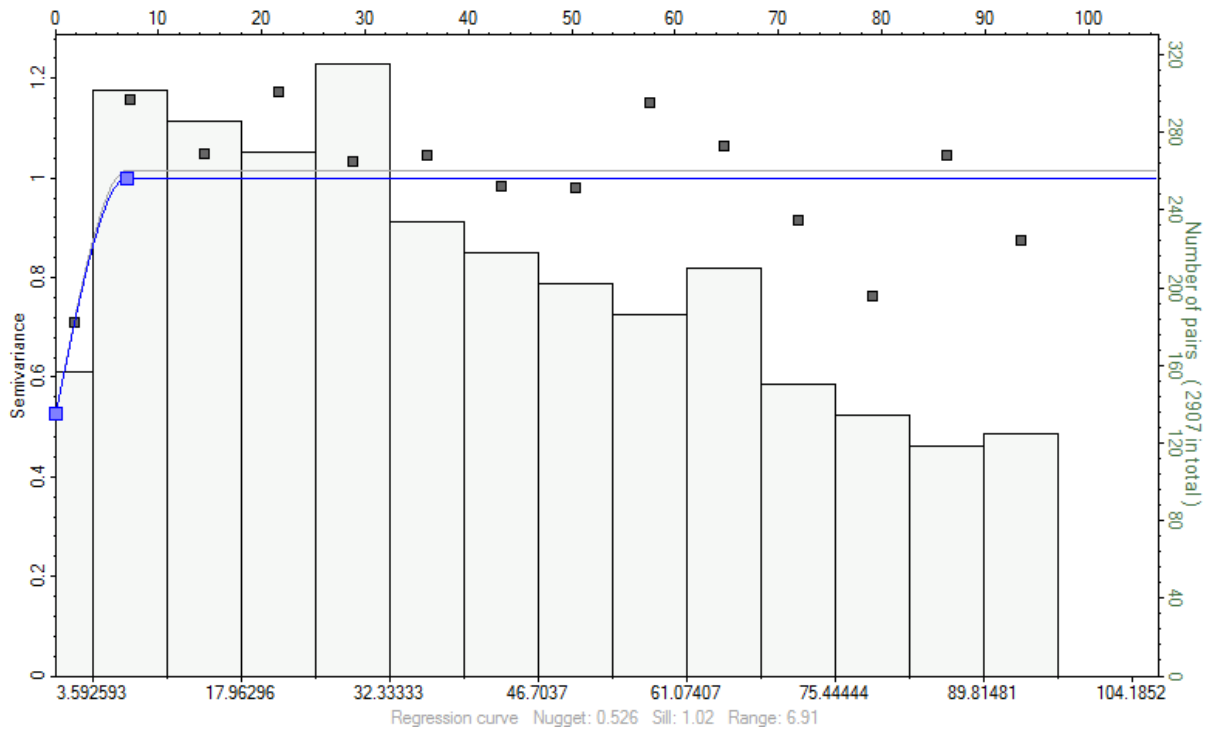


Figure E4. Vertical indicator variogram with normalized sill computed for siltstone in the alternative multilayered trap with a lag distance of 7.2 m. Generated in Petrel using data provided by SGU.

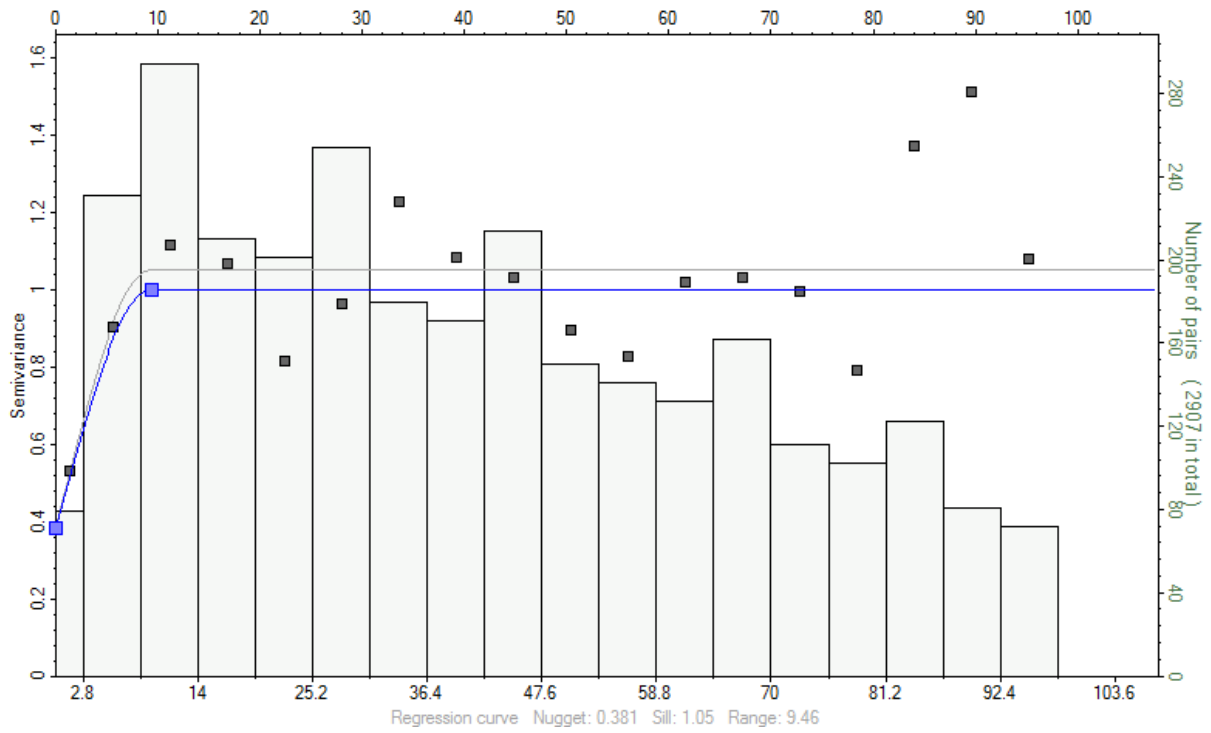


Figure E5. Vertical indicator variogram with normalized sill computed for fine-grained sandstone in the alternative multilayered trap with a lag distance of 5.6 m. Generated in Petrel using data provided by SGU.

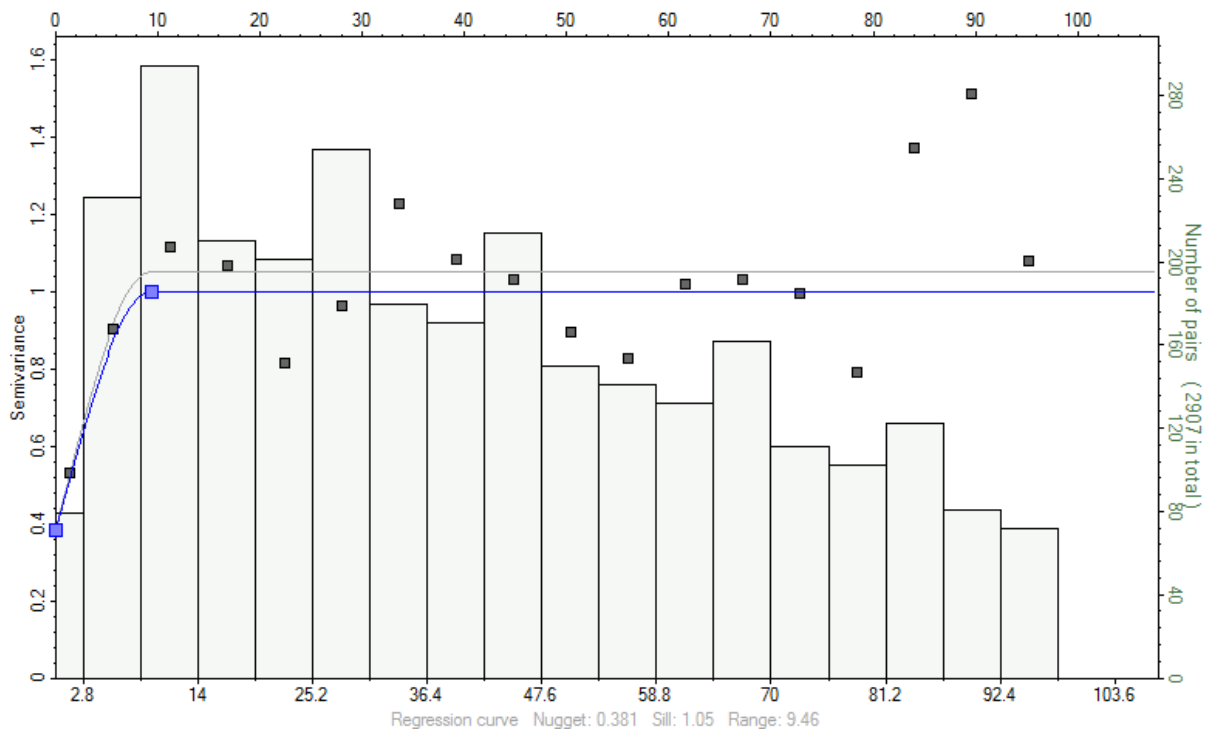


Figure E6. Vertical indicator variogram with normalized sill computed for medium-grained sandstone e in the alternative multilayered trap with a lag distance of 8.6 m. Generated in Petrel using data provided by SGU.